Hindawi Publishing Corporation
Advances in High Energy Physics
Volume 2013, Article ID 972485, 33 pages
http://dx.doi.org/10.1155/2013/972485

Review Article

Neutrino Propagation in Matter

Mattias Blennow[1,2] and Alexei Yu. Smirnov[3]

[1] *Division of Particle and Astroparticle Physics, Max-Planck-Institut für Kernphysik, Saupfercheckweg 1, 69117 Heidelberg, Germany*
[2] *Department of Theoretical Physics, KTH Royal Institute of Technology, AlbaNova University Center, Roslagstullsbacken 21, 106 91 Stockholm, Sweden*
[3] *High Energy, Cosmology and Astroparticle Physics Section, The Abdus Salam International Centre for Theoretical Physics, 34100 Trieste, Italy*

Correspondence should be addressed to Mattias Blennow; emb@kth.se

Received 3 August 2012; Accepted 21 November 2012

Academic Editor: Gian Luigi Fogli

We describe the effects of neutrino propagation in the matter of the Earth relevant to experiments with atmospheric and accelerator neutrinos and aimed at the determination of the neutrino mass hierarchy and CP violation. These include (i) the resonance enhancement of neutrino oscillations in matter with constant or nearly constant density, (ii) adiabatic conversion in matter with slowly changing density, (iii) parametric enhancement of oscillations in a multilayer medium, and (iv) oscillations in thin layers of matter. We present the results of semianalytic descriptions of flavor transitions for the cases of small density perturbations, in the limit of large densities and for small density widths. Neutrino oscillograms of the Earth and their structure after determination of the 1–3 mixing are described. A possibility to identify the neutrino mass hierarchy with the atmospheric neutrinos and multimegaton scale detectors having low energy thresholds is explored. The potential of future accelerator experiments to establish the hierarchy is outlined.

1. Introduction

Neutrinos are eternal travelers: once produced (especially at low energies) they have little chance to interact and be absorbed. Properties of neutrino fluxes are flavor compositions, lepton charge asymmetries, and energy spectra of encode information. Detection of the neutrinos brings unique knowledge about their sources, properties of medium, the space-time they propagated as well as about neutrinos themselves.

Neutrino propagation in matter is vast area of research which covers a variety of different aspects: from conceptual ones to applications. This includes propagation in matter (media) with (i) different properties (unpolarized, polarized, moving, turbulent, fluctuating, with neutrino components, etc.), (ii) different density profiles, and (iii) in different energy regions. The applications cover neutrino propagation in matter of the Earth and the Sun, supernova and relativistic jets as well as neutrinos in the early universe.

The impact of matter on neutrino oscillations was first studied by Wolfenstein in 1978 [1]. He marked that matter suppresses oscillations of the solar neutrinos propagating in the Sun and supernova neutrinos inside a star. He considered hypothetical experiments with neutrinos propagating through 1000 km of rock, something that today is no longer only a thought but actual experimental reality. Later Barger et al. [2] have observed that matter can also enhance oscillations at certain energies. The work of Wolfenstein was expanded upon in papers by Mikheev and Smirnov [3–5], in particular, in the context of the solar neutrino problem. Essentially two new effects have been proposed: the resonant enhancement of neutrino oscillations in matter with constant and nearly constant density and the adiabatic flavor conversion in matter with slowly changing density. It was marked that the first effect can be realized for neutrinos crossing the matter of the Earth. The second one can take place in propagation of solar neutrinos from the dense solar core via the resonance region inside the Sun to the surface with negligible density. This

adiabatic flavor transformation, called later the MSW effect, was proposed as a solution of the solar neutrino problem.

Since the appearance of these seminal papers, neutrino flavor evolution in background matter was studied extensively including the treatment of propagation in media which are not consisting simply of matter at rest, but also backgrounds that take on a more general form. For instance, in a thermal field theory approach [6], effects of finite temperature and density can be taken readily into account. If neutrinos are dense enough, new type of effects can arise due to the neutrino background itself, causing a collective behavior in the flavor evolution. This type of effect could have a significant impact on neutrinos in the early universe and in central parts of collapsing stars.

There has been a great progress in treatments of neutrino conversion in matter, both from an analytical and a pure computational points of view. From the analytical side, the description of three-flavor neutrino oscillations in matter is given by a plethora of formulas containing information that may be hard to get a proper grasp of without introducing approximations. Luckily, given the parameter values inferred from experiments, various perturbation theories and series expansions in small parameters can be developed. In this paper we will explain the basic physical effects important for the current and next generation neutrino oscillation experiments and provide the relevant formalism. We present an updated picture of oscillations and conversion given the current knowledge on the neutrino oscillation parameters.

In this paper we focus mainly on aspects related to future experiments with atmospheric and accelerator neutrinos. The main goals of these experiments are to (i) establish the neutrino mass hierarchy, (ii) discover CP violation in the lepton sector and determination of the CP-violating phase, (iii) precisely measure the neutrino parameters, in particular, the deviation of 2-3 mixing from maximal, and (iv) search for sterile neutrinos and new neutrino interactions.

Accelerator and atmospheric neutrinos propagate in the matter of the Earth. Therefore we mainly concentrate on effects of neutrino propagation in the Earth, that is, in usual electrically neutral and nonrelativistic matter. We update existing results on effects of neutrino propagation in view of the recent determination of the 1–3 mixing.

The paper is organized as follows. In Section 2 we consider properties of neutrinos in matter, in particular, mixing in matter and effective masses (eigenvalues of the Hamiltonian); we derive equations which describe the propagation. Section 3 is devoted to various effects relevant to neutrino propagating in the Earth. We consider the properties of the oscillation/conversion probabilities in different channels. In Section 4 we explore the effects of the neutrino mass hierarchy and CP-violating phase on the atmospheric neutrino fluxes and neutrino beams from accelerators. Conclusions and outlook are presented in Section 5.

2. Neutrino Properties in Matter

We will consider the system of 3-flavor neutrinos, $\nu_f^T \equiv (\nu_e, \nu_\mu, \nu_\tau)$, mixed in vacuum:

$$\nu_f = U_{\mathrm{PMNS}} \nu_m. \tag{1}$$

Here U_{PMNS} is the Pontecorvo-Maki-Nakagawa-Sakata (PMNS) mixing matrix [7–9] and $\nu_m^T \equiv (\nu_1, \nu_2, \nu_3)$ is the vector of mass eigenstates with masses m_i $(i = 1, 2, 3)$. We will use the standard parameterization of the PMNS matrix,

$$U_{\mathrm{PMNS}} = U_{23}(\theta_{23})\, I_\delta U_{13}(\theta_{13})\, I_\delta^* U_{12}(\theta_{12}), \tag{2}$$

which is the most suitable for describing usual matter effects. In (2) $U_{ij}(\theta_{ij})$ are the matrices of rotations in the ij-planes with angles θ_{ij} and $I_\delta \equiv \mathrm{diag}(1, 1, e^\delta)$.

In vacuum the flavor evolution of these neutrinos is described by the Schrödinger-like equation

$$i\frac{d\nu_f}{dt} = \frac{MM^\dagger}{2E}\nu_f, \tag{3}$$

where M is the neutrino mass matrix in the flavor basis and E is the neutrino energy. Equation (3) is essentially a generalization of the equation $E \approx p + m^2/2E$ for a single ultrarelativistic particle. According to (3), the Hamiltonian in vacuum can be written as

$$H_0 = \frac{1}{2E} U_{\mathrm{PMNS}} M_{\mathrm{diag}}^2 U_{\mathrm{PMNS}}^\dagger, \tag{4}$$

where $M_{\mathrm{diag}}^2 \equiv M^\dagger M = \mathrm{diag}(m_1^2, m_2^2, m_3^2)$ and we take the masses m_i to be real (the term pI is omitted in (4) since it does not produce a phase difference).

2.1. Refraction and Matter Potentials. The effective potential for a neutrino in medium V_f can be computed as a forward scattering matrix element $V_f = \langle \Psi | H_{\mathrm{int}} | \Psi \rangle$. Here Ψ is the wave function of the system of neutrino and medium, and H_{int} is the Hamiltonian of interactions.

At low energies, the Hamiltonian H_{int} is the effective four-fermion Hamiltonian due to exchange of the W and Z bosons:

$$\begin{aligned} H_{\mathrm{int}} = {} & \frac{G_F}{\sqrt{2}} \overline{\nu} \gamma^\mu (1 - \gamma_5) \nu \\ & \times \left\{ \overline{e} \gamma_\mu (g_V + g_A \gamma_5) e + \overline{p} \gamma_\mu \left(g_V^p + g_A^p \gamma_5 \right) p \right. \\ & \left. + \overline{n} \gamma_\mu \left(g_V^n + g_A^n \gamma_5 \right) n \right\}, \end{aligned} \tag{5}$$

where g_V and g_A are the vector and axial vector coupling constants.

In the Standard Model the matrix of the potentials in the flavor basis is diagonal: $V_f = \mathrm{diag}(V_e, V_\mu, V_\tau, 0, \ldots)$.

For medium the matrix elements of vectorial components of vector current are proportional to velocity of particles of medium. The matrix elements of the axial vector current are proportional to spin vector. Therefore for nonrelativistic and unpolarized medium (as well as for an isotropic distribution of ultrarelativistic electrons) only the γ^0 component of the vector current gives a nonzero result, which is proportional to the number density of the corresponding particles. Furthermore, due to conservation of the vector current (CVC), the couplings g_V^p and g_V^n can be computed using the neutral current couplings of quarks. Thus, taking into account that, in the Standard Model, the neutral current couplings of

electrons and protons are equal and of opposite sign, their NC contributionscancel in electrically neutral medium. As a result, the potential for neutrino flavor ν_a is

$$V_a = \sqrt{2}G_F\left(\delta_{ae}n_e - \frac{1}{2}n_n\right), \tag{6}$$

where n_e and n_n are the densities of electrons and neutrons, respectively.

Only the difference of potentials has a physical meaning. Contribution of the neutral current scattering to V is the same for all active neutrinos. Since V_a ($a = \mu, \tau$, or a combination thereof) is due to the neutral current scattering, in a normal medium composed of protons neutrons (nuclei) and electrons, $V_\mu - V_\tau = 0$. Furthermore, the difference of the potentials for ν_e and ν_a is due to the charged current scattering of ν_e on electrons ($\nu_e e \to \nu_e e$) [1]:

$$V = V_e - V_a = \sqrt{2}G_F n_e. \tag{7}$$

The difference of potentials leads to the appearance of an additional phase difference in the neutrino system: $\phi_{\text{matter}} \equiv (V_e - V_a)t \approx Vx$. This determines the *refraction length*, the distance over which an additional "matter" phase equals 2π:

$$l_0 \equiv \frac{2\pi}{V_e - V_a} = \frac{\sqrt{2}\pi}{G_F n_e}. \tag{8}$$

Numerically,

$$l_0 = 1.6 \cdot 10^9 \text{cm}\ \frac{1\,\text{g/cm}^3}{n_e m_N}, \tag{9}$$

where m_N is the nucleon mass. The corresponding column density $d \equiv l_0 n_e = \sqrt{2}\pi/G_F$ is given by the Fermi coupling constant only.

For antineutrinos the potential has an opposite sign. Being zero in the lowest order the difference of potentials in the ν_μ-ν_τ system appears at a level of $10^{-5}V$ due to the radiative corrections [10]. Thus in the flavor basis in the lowest order in EW interactions the effect of medium on neutrinos is described by $\widehat{V} = \text{diag}(V_e, 0, 0)$ with V_e given in (7).

The potential has been computed for neutrinos in different types of media, such as polarized or heavily degenerate electrons, in [11–13].

2.2. Evolution Equation, Effective Hamiltonian, and Mixing in Matter

2.2.1. Wolfenstein Equation. In the flavor basis, the Hamiltonian in matter can be obtained by adding the interaction term to the vacuum Hamiltonian in vacuum [1, 3–5, 14, 15]:

$$H_f = \frac{1}{2E}U_{\text{PMNS}}M^2_{\text{diag}}U^\dagger_{\text{PMNS}} + \widehat{V}. \tag{10}$$

In (10) we have omitted irrelevant parts of the Hamiltonian proportional to the unit matrix. The Hamiltonian for antineutrinos can be obtained by the substitution

$$U \longrightarrow U^*, \qquad V \longrightarrow -V. \tag{11}$$

There are different derivations of the neutrino evolution equation in matter, in particular, strict derivations starting from the Dirac equation or derivation in the context of quantum field theory (see [16] and references therein).

Although the Hamiltonian H_f describes evolution in time, with the connection $x = vt \approx x = ct$, (12) can be rewritten as $id\nu_f/dx = (H_0 + \widehat{V})\nu_f$ with $V = V(x)$, so it can be used as an evolution equation in space.

Due to the strong hierarchy of Δm^2 and the smallness of 1–3 mixing, the results can be qualitatively understood and in many cases quantitatively described by reducing 3ν evolution to 2ν evolution. The reason is that the third neutrino effectively decouples and its effect can be considered as a perturbation. Of course, there are genuine 3ν phenomena such as CP violation, but even in this case the dynamics of evolution can be reduced effectively to the dynamics of evolution of 2ν systems. The evolution equation for two-flavor states, $\nu_f^T = (\nu_e, \nu_a)$, in matter is

$$i\frac{d\nu_f}{dt} = \left[\frac{\Delta m^2}{4E}\begin{pmatrix} -\cos 2\theta & \sin 2\theta \\ \sin 2\theta & \cos 2\theta \end{pmatrix} + \begin{pmatrix} \frac{1}{2}V_e & 0 \\ 0 & -\frac{1}{2}V_e \end{pmatrix}\right]\nu_f, \tag{12}$$

where the Hamiltonian is written in symmetric form.

2.3. Mixing and Eigenstates in Matter. The mixing in matter is defined with respect to ν_{im}—the eigenstates of the Hamiltonian in matter H_f.

As usual, the eigenstates are obtained from the equation

$$H_f\nu_{im} = H_{im}\nu_{im}, \tag{13}$$

where H_{im} are the eigenvalues of H_f. If the density and therefore H_f are constant, ν_{im} correspond to the eigenstates of propagation. Since $H_f \neq H_0$, the states ν_{im} differ from the mass states, ν_i. For low density $n \to 0$, the vacuum eigenstates are recovered: $\nu_{im} \to \nu_i$. If the density, and thus H_f change during neutrino propagation, ν_{im} and H_{im} should be considered as the eigenstates and eigenvalues of the instantaneous Hamiltonian: $H_f = H_f(x)$, $\nu_{im} = \nu_{im}(x)$, and $H_{im} = H_{im}(x)$. For $n \to 0$ we have $H_{im} \to m_i^2/2E$.

The mixing in matter is a generalization of the mixing in vacuum (1). Recall that the mixing matrix in vacuum connects the flavor neutrinos, ν_f, and the massive neutrinos, ν_{mass}. The latter are the eigenstates of Hamiltonian in vacuum: $\nu_H = \nu_{\text{mass}}$. Therefore, the mixing matrix in matter is defined as the matrix which relates the flavor states with the eigenstates of the Hamiltonian in matter $\nu_H^T = (\nu_{1m}, \nu_{2m}, \nu_{3m})$:

$$\nu_f = U^m\nu_H. \tag{14}$$

From (13) we find that

$$\nu^\dagger_{jm}H_f\nu_{im} = H_{im}\delta_{ji}. \tag{15}$$

Furthermore, the Hamiltonian can be represented in the flavor basis as

$$H_f = \sum_{\alpha\beta}H_{\alpha\beta}\nu_\alpha\nu^\dagger_\beta. \tag{16}$$

Inserting this expression as well as the relation $\nu_{jm} = U^{m*}_{\alpha j}\nu_\alpha$, which follows from (14), into (15) one obtains

$$\sum_{\alpha\beta} U^{m*}_{\alpha j} H_{\alpha\beta} U^m_{\beta i} = H_{im}\delta_{ji} \tag{17}$$

or in matrix form $U^{m\dagger} H_f U^m = H^{\text{diag}} = \text{diag}(H_{1m}, H_{2m}, H_{3m})$. Thus, the mixing matrix U^m can be found diagonalizing the full Hamiltonian. The columns of the mixing matrix, $U_i \equiv (U^m_{ei}, U^m_{\mu i}, U^m_{\tau i})$, are the eigenstates of the Hamiltonian H_f which correspond to the eigenvalues H_{im}. Indeed, it follows from (17) that $H_f U^m = U^m H^{\text{diag}}$.

Equation (14) can be inverted to $\nu_H = U^{m\dagger}\nu_f$, or in components $\nu_{im} = U^{m*}_{\alpha i}\nu_\alpha$, $\alpha = e, \mu, \tau$. According to this, the elements of mixing matrix determine the flavor content of the mass eigenstates so that $|U^m_{\alpha i}|^2$ gives the probability to find ν_α in a given eigenstate ν_{im}. Correspondingly, the elements of the PMNS matrix determine the flavor composition of the mass eigenstates in vacuum.

2.4. Mixing in the Two-Neutrino Case. In the 2ν case, there is single mixing angle in matter θ_m and the relations between the eigenstates in matter and the flavor states read

$$\begin{aligned} \nu_e &= \cos\theta_m \nu_{1m} + \sin\theta_m \nu_{2m}, \\ \nu_a &= \cos\theta_m \nu_{2m} - \sin\theta_m \nu_{1m}. \end{aligned} \tag{18}$$

The angle θ_m is obtained by diagonalization of the Hamiltonian (12) (see previous section):

$$\begin{aligned} \sin^2 2\theta_m &= \frac{1}{R}\sin^2 2\theta, \\ R &\equiv \left(\cos 2\theta - \frac{2VE}{\Delta m^2}\right)^2 + \sin^2 2\theta, \end{aligned} \tag{19}$$

where R is the *resonance factor*. In the limit $V \to 0$, the factor $R \to 1$ and the vacuum mixing are recovered. The difference of eigenvalues H_{im} equals

$$\omega_m \equiv H_{2m} - H_{1m} = \frac{\Delta m^2}{2E}\sqrt{R}. \tag{20}$$

This difference is also called the level splitting or oscillation frequency, which determines the oscillation length: $l_m = 2\pi/\omega_m$ (see Section 3.2).

The matter potential and Δm^2 always enter the mixing angle and other dimensionless quantities in the combination

$$\frac{2EV}{\Delta m^2} = \frac{l_\nu}{l_0}, \tag{21}$$

where l_0 is the refraction length. This is the origin of the "scaling" behavior of various characteristics of the flavor conversion probabilities. In terms of the mixing angle in matter the Hamiltonian can be rewritten in the following symmetric form:

$$H_f = \frac{\omega^m}{2}\begin{pmatrix} -\cos 2\theta_m & \sin 2\theta_m \\ \sin 2\theta_m & \cos 2\theta_m \end{pmatrix}. \tag{22}$$

2.4.1. Resonance and Level Crossing. According to (19) the effective mixing parameter in matter, $\sin^2 2\theta_m$, depends on the electron density and neutrino energy through the ratio (21) of the oscillation and refraction lengths, $x = l_\nu/l_0 \propto EV$. The dependence $\sin^2 2\theta_m(VE)$ for two different values of the vacuum mixing angle, corresponding to angles from the full three-flavor framework, is shown in Figure 1. The dependence of $\sin^2 2\theta_m$ on E has a resonant character [3]. At

$$l_\nu = l_0 \cos 2\theta \tag{23}$$

the mixing becomes maximal: $\sin^2 2\theta_m = 1$ ($R = \sin^2 2\theta$). The equality in (23) is called the *resonance condition* and it can be rewritten as $2EV = \Delta m^2 \cos 2\theta$. For small vacuum mixing the condition reads the following: oscillation length ≈ refraction length. The physical meaning of the resonance is that the eigenfrequency, which characterizes a system of mixed neutrinos, $\omega = 2\pi/l_\nu = \Delta m^2/2E$, coincides with the eigenfrequency of the medium, $2\pi/l_0 = 1/V$. The resonance condition (23) determines the resonance density

$$n_e^R = \frac{\Delta m^2}{2E}\frac{\cos 2\theta}{\sqrt{2}G_F}. \tag{24}$$

The width of resonance on the half of height (in the density scale) is given by $2\Delta n_e^R = 2n_e^R \tan 2\theta$. Similarly, for fixed n_e one can introduce the resonance energy and the width of resonance in the energy scale. The width can be rewritten as $\Delta n_e^R = n_0 \sin 2\theta$, where $n_0 \equiv \Delta m^2/2\sqrt{2}EG_F$. When the mixing approaches its maximalvalue: $\theta \to \pi/4$, the resonance shifts to zero density: $n_e^R \to 0$, and the width of the resonance increases converging to the fixed value: $\Delta n_e^R \to n_0$.

In a medium with varying density, the layer in which the density changes in the interval $n_e^R \pm \Delta n_e^R$ is called the resonance layer. In this layer the angle θ_m varies in the interval from $\pi/8$ to $3\pi/8$.

For $V \ll V_R$, the mixing angle is close to the vacuum angle: $\theta_m \approx \theta$, while for $V \gg V_R$, the angle becomes $\theta_m \approx \pi/2$ and the mixing is strongly suppressed. In the resonance region, the level splitting is minimal [17, 18], therefore the oscillation length, as the function of density, is maximal.

2.5. Mixing of 3 Neutrinos in Matter. To a large extent, knowledge of the eigenstates (mixing parameters) and eigenvalues of the instantaneous Hamiltonian in matter allows the determination of flavor evolution in most of the realistic situations (oscillations in matter of constant density, adiabatic conversion, and strong breaking of adiabaticity). The exact expressions for the eigenstates and eigenvalues [19, 20] are rather complicated and difficult to analyze. Therefore approximate expressions for the mixing angles and eigenvalues are usually used. They can be obtained performing an approximate diagonalization of H_f which relies on the strong hierarchy of the mass squared differences:

$$r_\Delta \equiv \frac{\Delta m^2_{21}}{\Delta m^2_{31}} \approx 0.03. \tag{25}$$

Without changing physics, the factor $I_{-\delta}$ in the mixing matrix can be eliminated by permuting it with U_{12} and redefining

the state ν_3. Therefore, in what follows, we use $U_{\rm PMNS} = U_{23} I_\delta U_{13} U_{12}$. Here we will describe the case of normal mass hierarchy: $\Delta m^2_{31} > 0$, $\Delta m^2_{32} > 0$. Subtracting from the Hamiltonian the matrix proportional to the unit matrix $m_1^2/2E\mathbf{I}$, we obtain

$$M^2_{\rm diag} = \Delta m^2_{31}\,\mathrm{diag}\,(0, r_\Delta, 1)\,. \tag{26}$$

2.5.1. Propagation Basis. The propagation basis, $\widetilde{\nu} = (\nu_e, \widetilde{\nu}_2, \widetilde{\nu}_3)^T$, which is most suitable for consideration of the neutrino oscillations in matter, is defined through the relation

$$\nu_f = U_{23} I_\delta \widetilde{\nu}. \tag{27}$$

Since the potential matrix is invariant under 2-3 rotations, the matrix of the potentials is unchanged and the Hamiltonian in the propagation basis becomes

$$\widetilde{H} = \frac{1}{2E} U_{13} U_{12} M^2_{\rm diag} U^\dagger_{12} U^\dagger_{13} + \widehat{V}. \tag{28}$$

It does not depend on the 2-3 mixing or CP violation phase, and so the dynamics of the flavor evolution do not depend on δ and θ_{23}. These parameters appear in the final amplitudes when projecting the flavor states onto propagation-basis states and back onto (27) the neutrino production and detection.

Explicitly, the Hamiltonian $\widetilde{H}$ can be written as

$$\widetilde{H} = \frac{\Delta m^2_{31}}{2E} \times \begin{pmatrix} s^2_{13} + s^2_{12}\, c^2_{13}\, r_\Delta + \dfrac{2V_e E}{\Delta m^2_{31}} & s_{12}\, c_{12}\, c_{13}\, r_\Delta & s_{13}\, c_{13}\,(1 - s^2_{12}\, r_\Delta) \\ \cdots & c^2_{12}\, r_\Delta & -s_{12}\, c_{12}\, s_{13}\, r_\Delta \\ \cdots & \cdots & c^2_{13} + s^2_{12}\, s^2_{13}\, r_\Delta \end{pmatrix}. \tag{29}$$

Here all the off-diagonal elements contain small parameters r_Δ and/or s_{13}. Notice that, for the measured oscillation parameters, $s^2_{13} \sim r_\Delta$.

2.5.2. Mixing Angles in Matter. The Hamiltonian in (29) can be diagonalized performing several consecutive rotations which correspond to developing the perturbation theory in r_Δ. After a 1–3 rotation

$$\widetilde{\nu} = U_{13}\left(\theta^m_{13}\right)\nu' \tag{30}$$

over the angle θ^m_{13} determined by

$$\tan 2\theta^m_{13} = \frac{\sin 2\theta_{13}}{\cos 2\theta_{13} - 2EV'/\Delta m^2_{31}}, \quad \text{where} \quad V' = \frac{V}{1 - s^2_{12} r_\Delta}, \tag{31}$$

the 1–3 element of (29) vanishes. The expression (31) differs from that for 2ν mixing in matter by a factor $(1 - s^2_{12} r_\Delta)$, which increases the potential and deviates from 1 by

$$\xi \equiv s^2_{12} r_\Delta \approx 10^{-2}. \tag{32}$$

After this rotation the Hamiltonian in the ν' basis (30) becomes

$$H' = \frac{\Delta m^2_{31}}{2E} \times \begin{pmatrix} h_{11} & s_{12}\, c_{12}\, r_\Delta \cos\left(\theta^m_{13} - \theta_{13}\right) & 0 \\ \cdots & c^2_{12}\, r_\Delta & s_{12}\, c_{12} r_\Delta \sin\left(\theta^m_{13} - \theta_{13}\right) \\ \cdots & \cdots & h_{33} \end{pmatrix}, \tag{33}$$

where

$$h_{11,33} = \frac{1}{2}\left[\,(1 + \xi + x) \mp \sqrt{\left[\cos 2\theta_{13}\,(1 - \xi) - x\right]^2 + \sin^2 2\theta_{13}(1 - \xi)^2}\,\right], \tag{34}$$

and $x \equiv 2EV/\Delta m^2_{31}$. For $\xi = 0$, these elements are reduced to the standard 2ν expressions. In the limit of zero density, $x \to 0$, $h_{11} = \xi = s^2_{12} r_\Delta$, and consequently the 11-element of the Hamiltonian equals $H'_{11} = s^2_{12}\Delta m^2_{12}/2E$.

In the lowest r_Δ approximation one can neglect the nonzero 2-3 element in (33). The state ν'_3 then decouples and the problem is reduced to a two-neutrino problem for (ν'_1, ν'_2). The eigenvalue of this decoupled state equals

$$H_{3m} \approx \frac{\Delta m^2_{31}}{2E} h_{33}, \quad h_{33} \geq 1. \tag{35}$$

The diagonalization of the remaining 1-2 submatrix is given by rotation

$$\nu' = U_{12}\left(\theta^m_{12}\right)\nu_m, \tag{36}$$

where θ^m_{12} is determined by

$$\tan 2\theta^m_{12} = \frac{\sin 2\theta_{12} r_\Delta \cos\left(\theta^m_{13} - \theta_{13}\right)}{c^2_{12} r_\Delta - h_{11}}. \tag{37}$$

Here h_{11} and θ^m_{13} are defined in (34) and (31), respectively. The eigenvalues equal

$$H_{1m,2m} = \frac{\Delta m^2_{31}}{4E}\left[c^2_{12} r_\Delta + h_{11} \mp \sqrt{\left(c^2_{12} r_\Delta - h_{11}\right)^2 + \sin^2 2\theta_{12} r^2_\Delta \cos^2\left(\theta^m_{13} - \theta_{13}\right)}\,\right]. \tag{38}$$

According to this diagonalization procedure in the lowest order in r_Δ the mixing matrix in matter is given by

$$U^m = U_{23}\left(\theta_{23}\right) I_\delta U_{13}\left(\theta^m_{13}\right) U_{12}\left(\theta^m_{12}\right), \tag{39}$$

where mixing angles θ^m_{12} and θ^m_{13} are determined in (37) and (31), respectively. The 2-3 angle and the CP violation

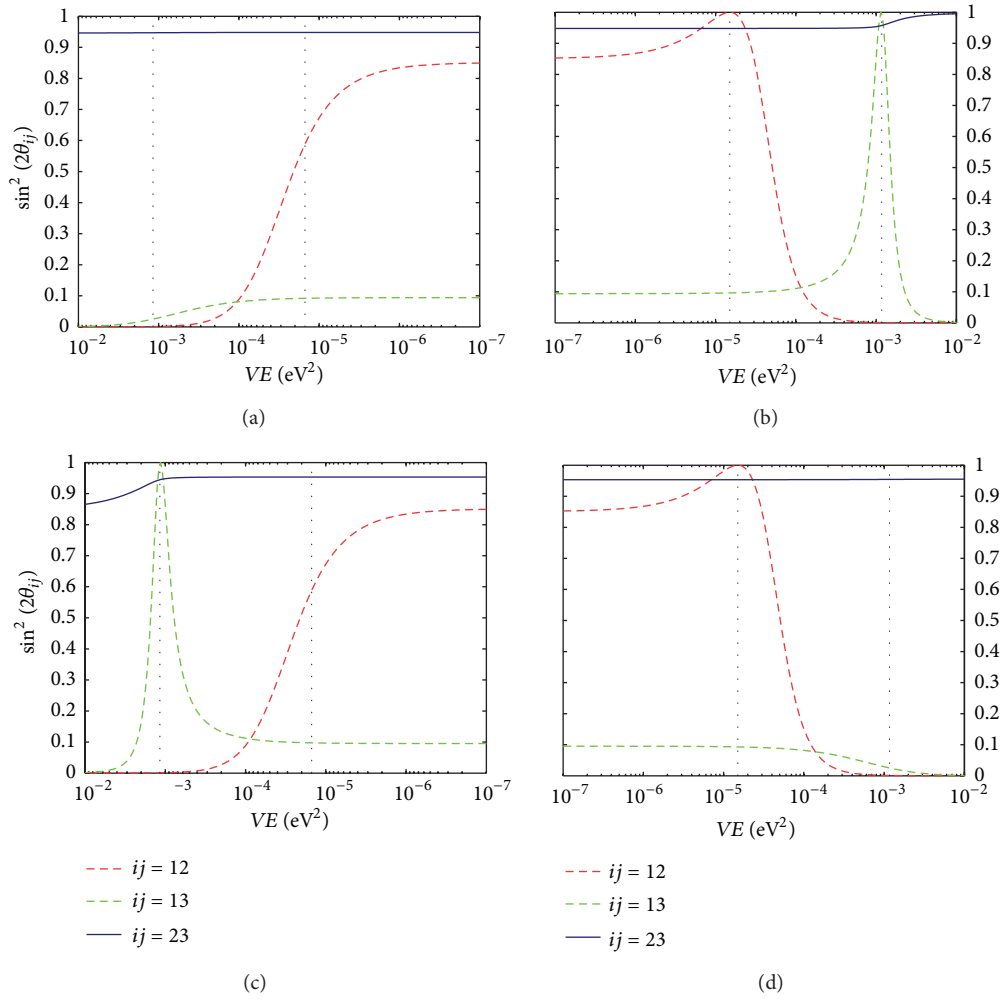

FIGURE 1: Resonance in neutrino mixing. The dependence of $\sin^2 2\theta_{mij}$ on the product VE for vacuum mixing: $\sin^2 2\theta_{12} = 0.851$, $\Delta m^2_{21} = 7.59 \cdot 10^{-5}$ eV^2 (red) and $\sin^2\theta_{13} = 0.0241$, $\Delta m^2_{31} = 2.47 \cdot 10^{-3}$ eV^2 (green). The left semiplane corresponds to antineutrinos. The behavior of θ_{23} with vacuum value $\sin^2 2\theta_{23} = 0.953$ is included for completeness. The dashed lines are the predictions from a strict two-flavor approximation while the solid thin lines are the results of numerical diagonalization of the full three-flavor system. The upper panels show the case of the normal mass hierarchy and the lower panels show the inverted hierarchy.

phase are not modified by matter in this approximation. The eigenvalues H_{1m} and H_{2m} are given in (38) and H_{3m} is determined by (35).

The 2-3 element of matrix (33) vanishes after additional 2-3 rotation by an angle $\theta'_{23} \sim r_\Delta$:

$$\tan 2\theta'_{23} = \frac{\sin 2\theta_{12}\ r_\Delta \sin\left(\theta^m_{13} - \theta_{13}\right)}{h_{33} - c^2_{12} r_\Delta}, \tag{40}$$

which produces corrections of the next order in r_Δ. With an additional 2-3 rotation the mixing matrix becomes

$$\begin{aligned} U^m &= U_{23}\left(\theta_{23}\right) I_\delta U_{13}\left(\theta^m_{13}\right) U_{12}\left(\theta^m_{12}\right) U_{23}\left(\theta'_{23}\right) \\ &\approx U_{23}\left(\theta^m_{23}\right) I_{\delta^m} U_{13}\left(\theta^m_{13}\right) U_{12}\left(\theta^m_{12}\right), \end{aligned} \tag{41}$$

where

$$U_{23}\left(\theta^m_{23}\right) I^m_\delta = U_{23}\left(\theta_{23}\right) I_\delta U_{23}\left(\bar\theta_{23}\right), \tag{42}$$

and the last 2-3 rotation is on the angle $\bar\theta_{23}$ determined through $\sin\bar\theta_{23} = \sin\theta'_{23}/\cos\theta^m_{13}$. The expression on the RH of (41) is obtained by reducing the expression on the LH side to the standard form by permuting the correction matrix $U_{23}(\theta'_{23})$. According to (42), it is this matrix that leads to the modification of 2-3 mixing and CP phase in matter. From (42) one finds

$$\sin\delta^m \sin 2\theta^m_{23} = \sin\delta \sin 2\theta_{23}, \tag{43}$$

that is, the combination $\sin\delta \sin 2\theta_{23}$ is invariant under inclusion of matter effects. Furthermore, $\theta^m_{23} \approx \theta_{23}$ and $\delta^m \approx \delta$ up to corrections of the order $O(r_\Delta)$. The results described here allowing understand the behavior of the mixing parameters $\sin^2 2\theta_{mij}$ in the EV region of the 1–3 resonance and above it (see Figure 1).

In Figure 2 we present dependence of the flavor content of the neutrino eigenstates on the potential. The energy level

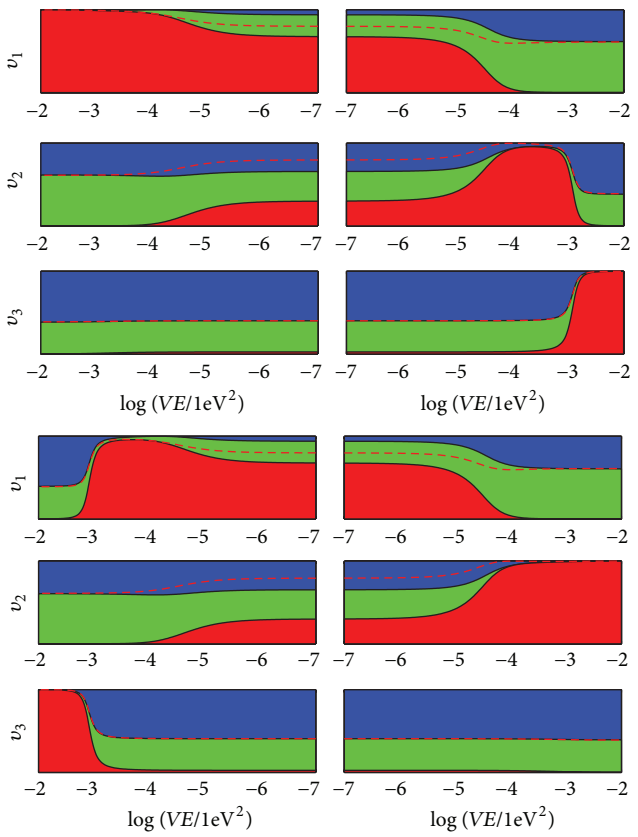

FIGURE 2: The flavor contents of the eigenstates of the Hamiltonian in matter as functions of EV. The vertical width of the band is taken to be 1, then the vertical sizes of the colored parts give $|U_{ei}|^2$ (red), and $|U_{\mu i}|^2$ (green), $|U_{\tau i}|^2$ (blue). The right and left panels correspond to neutrinos and antineutrinos, respectively. We take the best fit values of [21] with $\delta = 0$. Variations of δ change the relative ν_μ and $\nu_\tau$contents. The dashed red line shows a shift of border between ν_μ and ν_τ flavors for $\delta = \pi$. The upper (lower) panel corresponds to normal (inverted) mass ordering.

scheme, the dependence of the eigenvalues H_{im} on matter density, is shown in Figure 3. The energy levels in matter do not depend on δ or θ_{23}, but they do depend on the 1–3 and 1-2 mixing.

In the case of normal mass hierarchy, there are two resonances (level crossings) whose location is defined as the density (energy) at which the mixing in a given channel becomes maximal.

(1) The H resonance, in the ν_e-ν'_τ channel, is associated to the 1–3 mixing and large mass splitting. According to (31) $\theta^m_{13} = \pi/4$ at

$$V^R_{13} = \cos 2\theta_{13}\left(1 - s^2_{12} r_\Delta\right)\frac{\Delta m^2_{31}}{2E}. \tag{44}$$

(2) The L resonance at low densities is associated to the small mass splitting and 1-2 mixing. It appears in the ν'_e-ν'_μ channel, where ν'_e and ν_e differ by small (at low densities) rotation given by an angle $\sim \theta_{13}$ (see (31)). According to (37) the position of the L-resonance, $\theta^m_{12} = \pi/4$, is given by $c^2_{12} r_\Delta = h_{11}$, where h_{11} is defined in (34). This leads to

$$V^R_{12} = \cos 2\theta_{12}\frac{\Delta m^2_{21}}{2E}\frac{1}{c^2_{13}}. \tag{45}$$

For antineutrinos ($VE < 0$ in Figure 3), the oscillation parameters in matter can be obtained from the neutrino parameters taking $V \to -V$ and $\delta \to -\delta$. The mixing pattern and level scheme for neutrinos and antineutrinos are different both due to the possible fundamental violation of CP invariance and the sign of matter effect. Matter violates CP invariance and the origin of this violation stems from the fact that usual matter is CP asymmetric; in particular, there are electrons in the medium but no positrons.

In the case of normal mass hierarchy there are no antineutrino resonances (level crossings), and with the increase of density (energy) the eigenvalues have the following asymptotic limits:

$$H_{1m} \longrightarrow -V, \qquad H_{2m} \longrightarrow \frac{\Delta m^2_{21} c^2_{12}}{2E_\nu}, \qquad H_{3m} \longrightarrow \frac{\Delta m^2_{31} c^2_{13}}{2E_\nu}. \tag{46}$$

3. Effects of Neutrino Propagation in Different Media

3.1. The Evolution Matrix. The evolution matrix, $S(t, t_0)$, is defined as the matrix which gives the wave function of the neutrino system $\nu(t)$ at an arbitrary moment t once it is known in the initial moment t_0:

$$\nu(t) = S(t, t_0)\,\nu(t_0). \tag{47}$$

Inserting this expression in the evolution equation (12), we find that $S(t, t_0)$ satisfies the same evolution equation as $\nu(t)$:

$$i\frac{dS}{dt} = HS. \tag{48}$$

The elements $S(t, t_0)_{\alpha\beta}$ of this matrix are the amplitudes of $\nu_\beta \to \nu_\alpha$ transitions: $S(t, t_0)_{\alpha\beta} \equiv A(\nu_\beta \to \nu_\alpha)$. The transition probability equals $P_{\alpha\beta} = |S(t, t_0)_{\alpha\beta}|^2$. The unitarity of the evolution matrix, $S^\dagger S = I$, leads to the following relations between the amplitudes (matrix elements):

$$\begin{aligned} |S_{\alpha\alpha}|^2 + |S_{\beta\alpha}|^2 &= 1, \\ |S_{\beta\beta}|^2 + |S_{\alpha\beta}|^2 &= 1, \\ S^*_{\alpha\alpha} S_{\alpha\beta} + S^*_{\beta\alpha} S_{\beta\beta} &= 0, \\ S^*_{\alpha\beta} S_{\alpha\alpha} + S^*_{\beta\beta} S_{\beta\alpha} &= 0. \end{aligned} \tag{49}$$

The first and the second equations express the fact that the total probability of transition of ν_α to everything is one, and

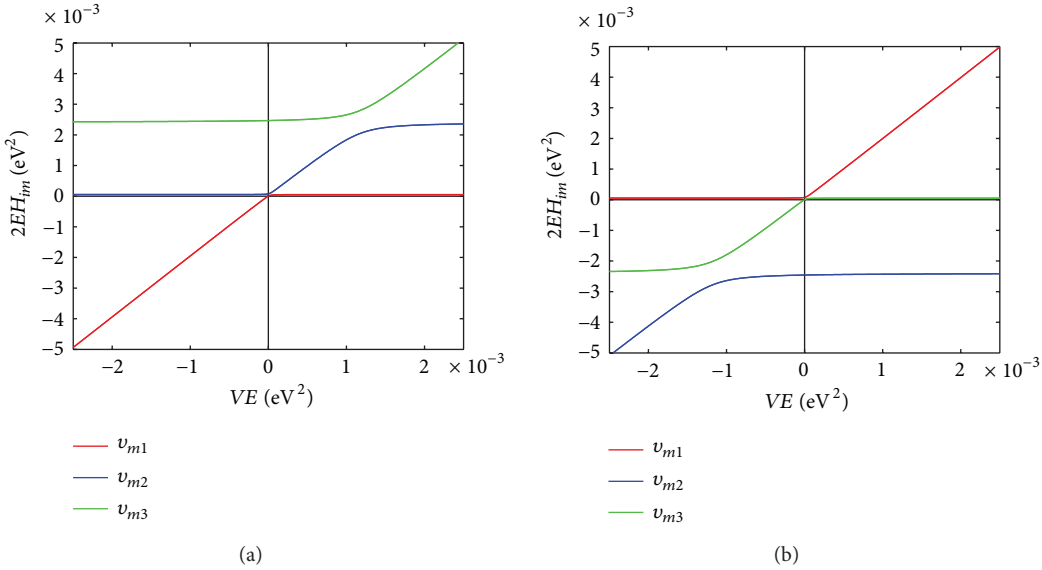

FIGURE 3: The energy level scheme. We here show the dependence of the eigenvalues of the Hamiltonian in matter on EV. Note that we are plotting $2EH_{im}$, which goes to Δm^2_{i1} for low VE. The left (right) panel corresponds to normal (inverted) mass ordering.

the same holds for ν_β. The third and fourth equations are satisfied if

$$S_{\alpha\alpha} = S^*_{\beta\beta}, \qquad S_{\beta\alpha} = -S^*_{\alpha\beta}. \tag{50}$$

With these relations the evolution matrix can be parametrized as

$$S = \begin{pmatrix} \alpha & \beta \\ -\beta^* & \alpha^* \end{pmatrix}, \qquad |\alpha|^2 + |\beta|^2 = 1. \tag{51}$$

The Hamiltonian for a 2ν system is T symmetric in vacuum as well as in medium with constant density. In medium with varying density the T symmetry is realized if the potential is symmetric. Under T transformations $S_{\beta\alpha} \to S_{\alpha\beta}$, and the diagonal elements $S_{\alpha\alpha}$ do not change. Therefore according to (50) the T invariance implies that $S_{\beta\alpha} = -S^*_{\beta\alpha}$, or $\mathrm{Re}\, S_{\beta\alpha} = 0$; that is, the off-diagonal elements of the S matrix are pure imaginary.

3.2. Neutrino Oscillations in Matter with Constant Density. In a medium with constant density and therefore constant potential the mixing is constant: $\theta_m(E, n) = \text{const}$. Consequently, the flavor composition of the eigenstates does not change and the eigenvalues H_{im} of the full Hamiltonian are constant. The two-neutrino evolution equation in matter of constant density can be written in the matter eigenstate basis as

$$i\frac{d\nu_m}{dx} = H^{\mathrm{diag}}\nu_m, \tag{52}$$

where $H^{\mathrm{diag}} \equiv \mathrm{diag}(H_{1m}, H_{2m})$. This system of equations splits and the integration is trivial, $\nu_{im}(t) = e^{-iH_{im}t}\nu_{im}(0)$. The corresponding S matrix is diagonal:

$$\widetilde{S}(x,0) = \begin{pmatrix} e^{i\phi_m(x)} & 0 \\ 0 & e^{-i\phi_m(x)} \end{pmatrix}, \tag{53}$$

where $\phi_m \equiv (1/2)\omega^m x$ is the half-oscillation phase in matter and a matrix proportional to the unit matrix has been subtracted from the Hamiltonian.

The S matrix in the flavor basis (ν_e, ν_a) is therefore

$$\begin{aligned} S(x,0) &= U^m \widetilde{S}(x,0)\, U^{m\dagger} \\ &= \begin{pmatrix} \cos\phi_m + i\cos 2\theta_m \ \sin\phi_m & -i\sin 2\theta_m \ \sin\phi_m \\ -i\sin 2\theta_m \ \sin\phi_m & \cos\phi - i\cos 2\theta_m \ \sin\phi_m \end{pmatrix}. \end{aligned} \tag{54}$$

Then, for the transition probability, we can immediately deduce

$$P_{ea} = |S_{ea}|^2 = \sin^2 2\theta_m \sin^2\phi_m, \tag{55}$$

where $\phi_m = \pi x/l_m$, with

$$l_m = \frac{2\pi}{H_{2m} - H_{1m}} = \frac{l_\nu}{\sqrt{R}} \tag{56}$$

being the oscillation length in matter. The dependence of l_m on the neutrino energy is shown in Figure 4. For small energies, $VE \ll \Delta m^2$, the length $l_m \simeq l_\nu$. It then increases with energy and for small θ reaches the maximum $l_m^{\max} = l_0/\sin 2\theta$ at $E^{\max} = E_R/\cos^2 2\theta$, that is, above the resonance energy. For $E \to \infty$ the oscillation length converges to the refraction length $l_m \to l_0$.

A useful representation of the S matrix for a layer with constant density follows from (54):

$$S(x,0) = \cos\phi_m I - i\sin\phi_m\,(\sigma\cdot\mathbf{n}), \tag{57}$$

where σ is a vector containing the Pauli matrices and $\mathbf{n} \equiv (\sin 2\theta_m, 0, -\cos 2\theta_m)$.

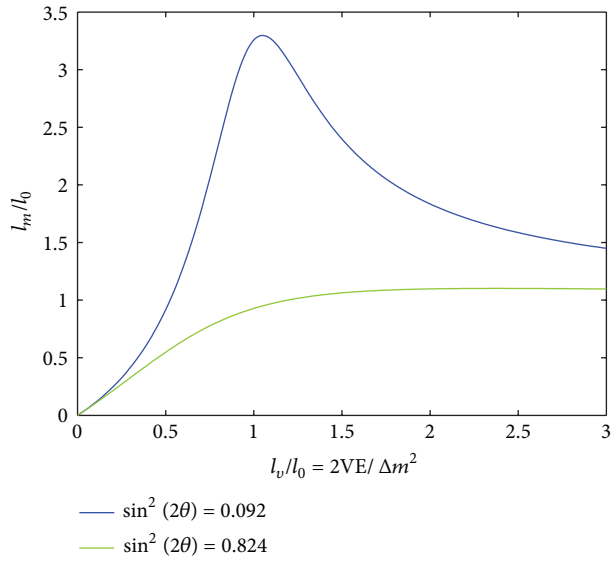

FIGURE 4: Dependence of the oscillation length in matter in units of the refraction length on neutrino energy for two different mixing angles in vacuum.

The dynamics of neutrino flavor evolution in uniform matter are the same as in vacuum, that is, it has a character of oscillations. However, the oscillation parameters (length and depth) differ from those in vacuum. They are now determined by the mixing and effective energy splitting in matter: $\sin^2 2\theta \to \sin^2 2\theta_m, l_\nu \to l_m$.

3.3. Neutrino Polarization Vectors and Graphic Representation. It is illuminating to consider the dynamics of transitions in different media using graphic representation [22–24]. Consider the two-flavor neutrino state, $\psi^T = (\psi_e, \psi_a)$. The corresponding Hamiltonian can be written as

$$H = (\mathbf{H} \cdot \sigma), \tag{58}$$

where $\sigma = (\sigma_1, \sigma_2, \sigma_3)$, $\mathbf{H}$ is the Hamiltonian vector $\mathbf{H} \equiv (2\pi/l_m) \cdot (\sin 2\theta_m, 0, \cos 2\theta_m)$, and $l_m = 2\pi/\Delta H_m$ is the oscillation length. The evolution equation then becomes

$$i\dot{\psi} = (\mathbf{H} \cdot \sigma)\,\psi. \tag{59}$$

Let us define the polarization vector $\mathbf{P}$

$$\mathbf{P} \equiv \psi^\dagger \frac{\sigma}{2} \psi. \tag{60}$$

In terms of the wave functions, the components of $\mathbf{P}$ equal

$$\begin{aligned} &\left(P_x, P_y, P_z\right) \\ &\quad = \left(\operatorname{Re} \psi_e^* \psi_a, \operatorname{Im} \psi_e^* \psi_a, \frac{1}{2}\left(|\psi_e|^2 - |\psi_a|^2\right)\right). \end{aligned} \tag{61}$$

The z-component can be rewritten as $P_z = |\psi_e|^2 - 1/2$; therefore $P_e \equiv |\psi_e|^2 = P_z + 1/2$ and from unitarity $P_a \equiv |\psi_a|^2 = 1/2 - P_z$. Hence, P_z determines the probabilities to find the neutrino in a given flavor state. The flavor evolution of the neutrino state corresponds to a motion of the polarization vector in the flavor space. The evolution equation for $\mathbf{P}$ can be obtained by differentiating (60) with respect to time and inserting $\dot{\psi}$ and $\dot{\psi}^\dagger$ from evolution equation (59). As a result, one finds that

$$\frac{d}{dt}\mathbf{P} = \mathbf{H} \times \mathbf{P}. \tag{62}$$

If $\mathbf{H}$ is identified with the strength of a magnetic field, the equation of motion (62) coincides with the equation of motion for the spin of electron in the magnetic field. According to this equation $\mathbf{P}$ precesses around $\mathbf{H}$.

With an increase of the oscillation phase ϕ (see Figure 5) the vector $\mathbf{P}$ moves on the surface of the cone having axis $\mathbf{H}$. The cone angle θ_a, the angle between $\mathbf{P}$ and $\mathbf{H}$, depends both on the mixing angle and on the initial state, and, in general, on changes in process of evolution, for example, if the neutrino evolves through several layers of different density. If the initial state is ν_e, the angle equals $\theta_a = 2\theta_m$ in the initial moment.

The components of the polarization vector $\mathbf{P}$ are nothing but the elements of the density matrix $\rho = \sigma \cdot \mathbf{P}$. The evolution equation for ρ can be obtained from (62)

$$i\frac{d\rho}{dt} = [H, \rho]. \tag{63}$$

The diagonal elements of the density matrix give the probabilities to find the neutrino in the corresponding flavor state.

3.4. Resonance Enhancement of Oscillations. Suppose a source produces flux of neutrinos in the flavor state ν_μ with continuous energy spectrum. This flux then traverses a layer of length L with constant density n_e. At the end of this layer a detector measures the ν_e component of the flux, so that oscillation effect is given by the transition probability $P_{\mu e}$. In Figure 6 we show dependence of this probability on

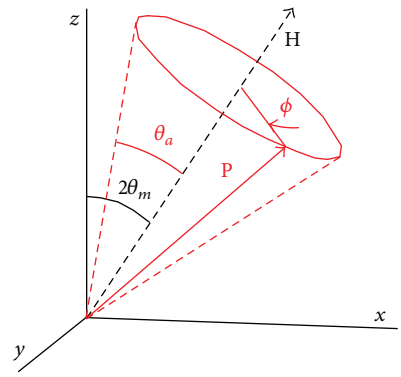

FIGURE 5: Graphic representation of neutrino oscillations. Neutrino polarization vector **P** precesses around the Hamiltonian vector **H** (or the vector of eigenstates of the Hamiltonian). The angle between **P** and **H** is given by the cone angle θ_a, and the direction of axis of the cone is determined by the mixing angle in matter $2\theta_m$.

energy for thin and thick layers. The oscillatory curves are inscribed in the resonance envelope $\sin^2 2\theta_m$. The period of the oscillatory curve decreases with the length L. At the resonance energy,

$$E_R = \frac{\Delta m^2 \cos 2\theta}{2V} = \frac{\Delta m^2 \cos 2\theta}{2\sqrt{2} G_F n_e}, \tag{64}$$

oscillations proceed with maximal depths. Oscillations are enhanced up to $P > 1/2$ in the resonance range $(E_R \pm \Delta E_R)$ where $\Delta E_R = \tan 2\theta E_R$ (see Section 2.4). This effect was called the resonance enhancement of oscillations.

3.5. Three-Neutrino Oscillations in Matter with Constant Density. The oscillation probabilities in matter with constant density have the same form as oscillation probabilities in vacuum and the generalization of (53) is straightforward. In the basis of the eigenstates of the Hamiltonian the evolution matrix equals

$$\widetilde{S}(x,0) = \begin{pmatrix} e^{-2i\phi_{1m}(x)} & 0 & 0 \\ 0 & e^{-2i\phi_{2m}(x)} & 0 \\ 0 & 0 & e^{-2i\phi_{3m}(x)} \end{pmatrix}, \tag{65}$$

and for the elements of the S matrix in the flavor basis we obtain $S_{\alpha\beta} = \sum_i U^{m*}_{\alpha i} U^m_{\beta i} e^{-2i\phi_i^m(x)}$. Removing $e^{-2i\phi_{2m}}$ and using the unitarity of the mixing matrix in matter we have

$$\begin{aligned} S_{\alpha\beta} = {} & \delta_{\alpha\beta} + 2ie^{\phi^m_{21}(x)} U^{m*}_{\alpha 2} U^m_{\beta 2} \sin\phi^m_{21}(x) \\ & - 2ie^{-i\phi^m_{32}(x)} U^{m*}_{\alpha 3} U^m_{\beta 3} \sin\phi^m_{32}(x). \end{aligned} \tag{66}$$

In particular, for the amplitudes in matter involving only ν_e and ν_μ, we obtain

$$\begin{aligned} S^{\text{cst}}_{e\mu} = {} & 2ie^{i\phi^m_{21}} \left[U^m_{e1} U^{m*}_{\mu 1} \sin\phi^m_{21} \right. \\ & \left. - e^{-i\phi^m_{31}} U^m_{e3} U^{m*}_{\mu 3} \sin\phi^m_{32} \right], \\ S^{\text{cst}}_{\mu\mu} = {} & 1 + 2ie^{i\phi^m_{21}} \left| U^m_{\mu 1} \right|^2 \sin\phi^m_{21} \\ & - 2ie^{-i\phi^m_{32}} \left| U^m_{\mu 3} \right|^2 \sin\phi^m_{32}, \\ S^{\text{cst}}_{ee} = {} & 1 + 2ie^{i\phi^m_{21}} \cos^2\theta^m_{13} \cos^2\theta^m_{12} \sin\phi^m_{21} \\ & - 2ie^{-i\phi^m_{32}} \sin^2\theta^m_{13} \sin\phi^m_{32}. \end{aligned} \tag{67}$$

3.6. Propagation in a Medium with Varying Density and the MSW Effect

3.6.1. Equation for the Instantaneous Eigenvalues and the Adiabaticity Condition. In nonuniform media, the density changes along neutrino trajectory: $n_e = n_e(t)$. Correspondingly, the Hamiltonian of system depends on time, $H = H(t)$, and therefore the mixing angle changes during neutrino propagation: $\theta_m = \theta_m(n_e(t))$. Furthermore, the eigenstates of the instantaneous Hamiltonian, ν_{1m} and ν_{2m}, are no longer the "eigenstates" of propagation. Indeed, inserting $\nu_f = U(\theta_m)\nu_m$ in the equation for the flavor states (c.f., (3)) we obtain the evolution equation for eigenstates ν_{im}:

$$i\frac{d\nu_m}{dt} = \begin{pmatrix} H_{1m} & -i\dot{\theta}_m \\ i\dot{\theta}_m & H_{2m} \end{pmatrix} \nu_m, \tag{68}$$

where $\dot{\theta}_m \equiv d\theta_m/dt$. The Hamiltonian for ν_{im} (68) is nondiagonal and, consequently, the transitions $\nu_{1m} \leftrightarrow \nu_{2m}$ occur. The rate of these transitions is given by the speed with which the mixing angle changes with time. According to (68) [3, 25], $|\dot{\theta}_m|$ determines the energy of transition $\nu_{1m} \leftrightarrow \nu_{2m}$ and $|H_{2m} - H_{1m}|$ gives the energy gap between the levels.

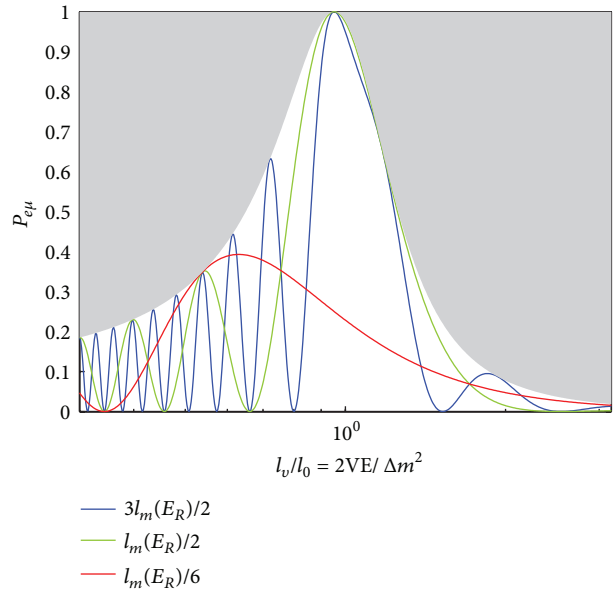

FIGURE 6: Resonance enhancement of neutrino oscillations in matter with constant density. Shown is the dependence of the transition probability $\nu_e \to \nu_\mu$ on energy for $\sin^2\theta_{13} = 0.0241$ for three different sizes of layers: $L = 3l_m(E_R)/2$, $l_m(E_R)/2$, and $l_m(E_R)/6$. The shaded area shows the resonance envelope: $\sin^2 2\theta_m(E)$.

The off-diagonal elements of the evolution equation (68) can be neglected if $\dot{\theta}_m$ is much smaller than other energy scales in the system. The difference of the diagonal elements of the Hamiltonian is, in fact, the only other energy quantity and therefore the criterion for smallness of $\dot{\theta}_m$ is

$$\dot{\theta}_m \ll H_{2m} - H_{1m}. \tag{69}$$

This inequality implies a slow enough change of density and is called the *adiabaticity condition*. Defining the adiabaticity parameter [22, 25] as

$$\gamma \equiv \left| \frac{\dot{\theta}_m}{H_{2m} - H_{1m}} \right|, \tag{70}$$

the adiabaticity condition can be written as $\gamma \ll 1$.

For small mixing angle, the adiabaticity condition is most crucial in the resonance layer where the level splitting is small and the mixing angle changes rapidly. In the resonance point, it takes the physically transparent form [3]: $\Delta r_R > l_m^R$, where $l_m^R \equiv l_\nu/\sin 2\theta$ is the oscillation length in resonance, and $\Delta r_R \equiv (n_e/(dn_e/dr))_R \tan 2\theta$ is the spatial width of the resonance layer. According to this condition at least one oscillation length should be obtained within the resonance layer.

In the case of large vacuum mixing, the point of maximal adiabaticity violation [26, 27] is shifted to density, $n_e(av)$, larger than the resonance density: $n_e(av) \to n_B > n_R$. Here $n_B = \Delta m^2/2\sqrt{2}G_F E$ is the density at the border of resonance layer for maximal mixing. Outside the resonance and in the nonresonant channel, the adiabaticity condition has been considered in [28, 29].

3.7. Adiabatic Conversion and the MSW Effect. If the adiabaticity condition is fulfilled and $\dot{\theta}_m$ can be neglected, the Hamiltonian for the eigenstates becomes diagonal. Consequently, the equations for the instantaneous eigenstates ν_{im} split as in the constant density case. The instantaneous eigenvalues evolve independently, but the flavor content of the eigenstates changes according to the change of mixing in matter. This is the essence of the adiabatic approximation; we neglect $\dot{\theta}_m$ in evolution equation but do not neglect the dependence of θ_m on density. The solution can be obtained immediately as

$$\begin{aligned} \widetilde{S}(x,0) &= \begin{pmatrix} e^{i\phi_m} & 0 \\ 0 & e^{-i\phi_m} \end{pmatrix}, \\ \phi_m &= \frac{1}{2}\int_0^x (H_{2m} - H_{1m})\, dx', \end{aligned} \tag{71}$$

in symmetric form. The only difference from the constant density case is that the eigenvalues now depend on time and therefore integration appears in the phase factors.

The evolution matrix in the flavor basis can be obtained by projecting back from the eigenstate basis to the flavor basis with the mixing matrices corresponding to initial and final densities:

$$\begin{aligned} &S_f(x,0) \\ &\quad = U^m(t)\,\widetilde{S}(x,0)\,U^{m\dagger}(0) \\ &\quad = \begin{pmatrix} c_m c_m^0 e^{i\phi_m} + s_m s_m^0 e^{-i\phi_m} & -c_m s_m^0 e^{i\phi_m} + s_m c_m^0 e^{-i\phi_m} \\ -s_m c_m^0 e^{i\phi_m} + c_m s_m^0 e^{-i\phi_m} & s_m s_m^0 e^{i\phi_m} + c_m c_m^0 e^{-i\phi_m} \end{pmatrix}. \end{aligned} \tag{72}$$

From this procedure we find, for example, the probability of ν_e-ν_e transition

$$P_{ee} = \left|S_f(x,0)_{ee}\right|^2 = \frac{1}{2}\left[1 + \cos 2\theta_m(x)\cos 2\theta_m(0)\right] + \frac{1}{2}\sin 2\theta_m(x)\sin 2\theta_m(0)\cos 2\phi_m(x). \quad (73)$$

If the initial and final densities coincide, as in the case of neutrinos crossing the Earth, we obtain the same formulas as in constant density case:

$$P_{\alpha\beta} = \left|\sum_i U^m_{\alpha i}(0)\, U^{m*}_{\beta i}(0)\, e^{-i\phi_{im}(t,0)}\right| \quad (74)$$

with the mixing angle taken at the borders (initial or final state). In particular, the survival probability equals $P_{\alpha\alpha} = 1 - \sin^2 2\theta_m(0)\sin^2\phi_m(x)$.

Averaging over the phase, which means that the contributions from ν_1 and ν_2 add incoherently, gives

$$P = \left(\cos\theta_m \cos\theta^0_m\right)^2 + \left(\sin\theta_m \sin\theta^0_m\right)^2 = \sin^2\theta_m + \cos 2\theta_m \cos^2\theta^0_m. \quad (75)$$

The mixing in the neutrino production point θ^0_m is determined by density in this point, n^0_e, and the resonance density. Consequently, the picture of the conversion depends on how far from the resonance layer (in the density scale) a neutrino is produced. Strong transitions occur if the initial and final mixings differ substantially, which is realized when the initial density is much above the resonance density and the final one is below the resonance density and therefore neutrinos cross the resonance layer.

According to (73) the oscillation depth equals $D = |\sin 2\theta_m \sin 2\theta^0_m|$. Both the averaged probability (75) and the depth (73) are determined by the initial and final densities and do not depend on the density distribution along the neutrino trajectory. Essentially they are determined by the ratios $y \equiv n/n_R$ in the initial and final moments. This is a manifestation of the universality of the adiabatic approximation result.

In contrast, the phase does depend on the density distribution and the period of oscillations (the latter is given by the oscillation length in matter). So, it is the phase that encodes information about the density distribution.

The probability depends on t via the phase $\phi_m(t)$ and also via the mixing angle $\theta_m(t)$. Two degrees of freedom are operative and P dependence on time is an interplay of two effects: oscillations, associated with the phase $\phi_m(t)$, and the adiabatic conversion related to change of θ_m. Depending on initial condition n^0_e, the relative importance of the two effects is different. If neutrinos are produced far above the resonance, $n^0_e \gg n^R_e$, the initial mixing is strongly suppressed, $\theta^0_m \approx \pi/2$. Consequently, the neutrino state, for example, ν_e, consists mainly of one eigenstate, ν_{2m}, and furthermore, one-flavor ν_e dominates in ν_{2m}. Since the admixture of the second eigenstate is very small, oscillations (interference effects) are strongly suppressed. Thus, here the nonoscillatory flavor transition occurs when the flavor of whole state (which nearly coincides with ν_{2m}) follows the density change. At zero density $\nu_{2m} = \nu_2$, and therefore the probability to find the electron neutrino (survival probability) equals [3]

$$P = \left|\langle \nu_e \mid \nu(t)\rangle\right|^2 \approx \left|\langle \nu_e \mid \nu_{2m}(t)\rangle\right|^2 = \left|\langle \nu_e \mid \nu_2\rangle\right|^2 \approx \sin^2\theta. \quad (76)$$

The final probability, $P = \sin^2\theta$, is the feature of the nonoscillatory transition (as pure adiabatic conversion). Deviation from this value indicates the presence of oscillations; see (73).

If neutrinos are produced not too far from resonance, for example, at $n^0_e > n^R_e$, the initial mixing is not suppressed. Although ν_{2m} is the main component of the neutrino state, the second eigenstate, ν_{1m}, has appreciable admixture; the flavor mixing in the neutrino eigenstates is significant, and the interference effect is not suppressed. Here we deal with the interplay of the adiabatic conversion and oscillations.

Production in the resonance is a special case; if $\theta^0_m = 45^\circ$, the averaged probability equals $\overline{P} = 1/2$ independently of the final mixing. This feature is important for determining the oscillation parameters. Strong transitions ($P > 1/2$) occur when neutrinos cross resonance layer. These features are realized for solar neutrinos when propagating from their production region inside the Sun to the surface of the Sun. The adiabatic propagation occurs also in a single layer of the Earth (e.g., in the mantle).

3.8. Adiabaticity Violation. For most of applications the adiabaticity is either well satisfied (neutrinos in the Sun or supernovae), or maximally broken due to sharp (instantaneous) density change (neutrinos in the Earth, neutrinos crossing the shock wave fronts in supernova). In the former case the evolution is described by the adiabatic formulas. In the latter case description is also simple; one just needs to match the flavor conditions at the borders between layers, find the flavor state before the density jump, and then use it as an initial state for the evolution after the jump. The intermediate case of the adiabaticity breaking can be realized for neutrinos in the mantle of the Earth, for high energy neutrinos propagating in the Sun (neutrinos from annihilation of hypothetical WIMPs) or for sterile neutrinos with very small mixing.

If the density changes rapidly, $\dot{\theta}_m$ is not negligible in (68) and the adiabaticity condition (70) is not satisfied. The transitions $\nu_{1m} \leftrightarrow \nu_{2m}$ become noticeable and therefore the admixtures of the eigenstates in a given propagating state change. The S matrix in the flavor basis is given by

$$S_f(x,0) = U^m(t)\,\widetilde{S}(x,0)\,U^{m\dagger}(0) = U^m(t)\begin{pmatrix} S_{11} & -S^*_{21} \\ S_{21} & S^*_{11}\end{pmatrix} U^{m\dagger}(0), \quad (77)$$

where $\widetilde{S}$ is the evolution matrix in the basis of instantaneous eigenstates. Then the ν_e-ν_e transition probability $P_{ee} \equiv |S_f(x,0)_{ee}|^2$ equals

$$P_{ee} = \frac{1}{2}\left[1 + \cos 2\theta_m(t)\cos 2\theta_m(0)\right] - P_{21}\cos 2\theta_m(t)\cos 2\theta_m(0) + P_{\text{int}}, \tag{78}$$

where $P_{21} \equiv |S_{21}|^2$ is the probability of $\nu_{2m} \to \nu_{1m}$ transitions and P_{int} is an interference term

$$P_{\text{int}} = \frac{1}{4}\sin 2\theta_m(t)\sin 2\theta_m(0)\left[S_{11}^2 + S_{11}^{*2} + S_{21}^2 + S_{21}^{*2}\right] + \frac{1}{2}\sin\left[2\theta_m(0) - 2\theta_m(x)\right]\left[S_{11}S_{21}^* + S_{11}^*S_{21}\right], \tag{79}$$

which depends on the oscillation phase. The averaged probability ($P_{\text{int}} = 0$) equals [30]

$$P_{ee} = \frac{1}{2} + \left(\frac{1}{2} - P_{21}\right)\cos 2\theta_m(t)\cos 2\theta_m(0). \tag{80}$$

If the initial density is much larger than the resonance density, then $\theta_m(0) \approx \pi/2$ and $\cos 2\theta_m(0) = -1$. In this case the averaged probability can be rewritten as

$$P_{ee} = \sin^2\theta_m(t) + P_{21}\cos 2\theta_m(t). \tag{81}$$

Violation of adiabaticity weakens transitions if $\cos 2\theta_m(t) > 0$, thus leading to an increase of the survival probability. In the adiabatic case $S_{11} = e^{i\phi_m}$, $S_{21} = 0$, and therefore $S_{11}^2 + S_{11}^{*2} = 2\cos 2\phi_m(x)$, so that (78) is reduced to (73).

In the graphic representation (Figure 5), the neutrino vector moves on the surface of the cone (phase change) and the axis of the cone rotates according to the density change. The cone angle θ_a changes as a result of violation of the adiabaticity).

There are different approaches to compute the flop probability P_{21}. In the adiabatic regime the probability of transition between the eigenstates is exponentially suppressed $P_{12} \sim \exp(-\pi/2\gamma)$ with γ given in (70) [30, 31]. One can consider such a transition as penetration through a barrier of height $H_{2m} - H_{1m}$ by a system with the kinetic energy $d\theta_m/dt$. This leads to the Landau-Zener probability

$$P_{LZ} = \exp\left(-\pi^2\kappa_R\right) = \exp\left(-\frac{\pi h\Delta m^2}{4E}\frac{\sin^2 2\theta}{\cos 2\theta}\right), \tag{82}$$

where $h \equiv n(dn/dr)^{-1}$ [32]. In the case of weak adiabaticity violation, one can develop an adiabatic perturbation theory which gives the results as a series expansion in the adiabaticity parameter [33].

3.9. Theory of Small Matter Effects

3.9.1. Minimal Width Condition. If the vacuum mixing angle is small, there exists a lower limit on the amount of matter needed to induce significant flavor change due to matter effect. The amount of matter is characterized by the column density of electrons along the neutrino trajectory:

$$d = \int_0^L n_e(x)\,dx. \tag{83}$$

We can define $d_{1/2}$ as the column density for which the oscillation transition probability surpasses 1/2 for the first time in the course of propagation. Then it is possible to show that [34]

$$d_{1/2} \geq d_{\min} = \frac{\pi}{2\sqrt{2}G_F\tan 2\theta} \tag{84}$$

for all density profiles. Furthermore, the minimum, $d_{\min}$, is realized for oscillations in a medium of constant density equal to the resonance density. The relation (84) is known as the minimal width condition. This condition originates from an interplay between matter effects and vacuum mixing. The acquired matter phase, $\sqrt{2}G_F d$, must be large. At the same time, since matter effects by themselves are flavor conserving, also vacuum mixing is required in order to induce flavor conversion. The smaller the vacuum mixing is, the larger the width that is required.

3.9.2. Vacuum Mimicking. Vacuum mimicking [35], which states that regardless of the matter density, the initial flavor evolution of neutrino state is similar to that of vacuum oscillations. Consequently for small baselines, L, it is not possible to see matter effect and any such effect appearing in higher order of L. Indeed, consider the evolution matrix

$$S = \mathcal{T}\left[\exp\left(-i\int_0^L H(x)\,dx\right)\right], \tag{85}$$

where $\mathcal{T}$ denotes time ordering of the exponential. For small values of L, it can be expanded as

$$S = 1 - i\int_0^L H(x)\,dx + \mathcal{O}\left(L^2\right). \tag{86}$$

If initial neutrino state has definite flavor, the amplitude of flavor transition is given by the off-diagonal element of $H(x)$ which does not depend on matter potential. The matter contribution to $H(x)$ is diagonal. Therefore the flavor transitions depend on the matter density only at higher order in L. This result holds true as long as $L \ll l_m$ or when the phase of oscillation is small [36].

This can be seen explicitly in the case of medium with constant density where, expanding the oscillatory factor for small oscillation phase, we have the transition probability

$$P = \sin^2 2\theta_m \sin^2\phi^m = \frac{1}{R}\sin^2 2\theta\sin^2\phi\sqrt{R} \approx \phi^2\sin^2 2\theta. \tag{87}$$

Note that vacuum mimicking only occurs if the initial neutrino state is a flavor eigenstate [36]. If the initial neutrino is in a flavor-mixed state, for example, in a mass eigenstate,

then matter will affect this state already at lowest order in L. This situation is realized in several settings involving astrophysical neutrinos propagating through the Earth, for example, solar and supernova neutrinos, where the neutrinos arrive at the Earth as mass eigenstates. The mimicking is not valid if there are nonstandard flavor changing interactions, so that matter effect appears in the off-diagonal elements of the Hamiltonian.

3.9.3. Effects of Small Layers of Matter. If the minimal width condition is not satisfied, that is $d = nx \ll G_F^{-1}$, the matter effect on result of evolution is small. This inequality can be written as $Vx \ll 1$ which means that the oscillation phase is small. In this case the matter effect can be considered as small perturbation of the vacuum oscillation result even if the MSW resonance condition is satisfied.

The reasons for the smallness of the matter effect are different depending on the energy interval. Consider a layer of constant density with the length x. There are three possibilities.

(i) $E \ll E_R$ (E_R is the resonance density)—nearly vacuum oscillations in low density medium take place. Matter effect gives small corrections to the oscillation depth and length which are characterized by $2VE/\Delta m^2 = Vx/2\pi \ll 1$, here $x \sim l_\nu$.

(ii) $E \sim E_R$—modification of oscillation parameters is strong; however $l_\nu^R \sim l_\nu/\sin 2\theta \sim 2\pi/(V \sin 2\theta)$. Consequently, $x/l_\nu^R = xV \sin 2\theta/2\pi \ll 1$. Oscillations are undeveloped due to smallness of phase.

(iii) $E \gg E_R$—matter suppresses oscillation depth by a factor $E_R/E \ll 1$. Since the oscillation length equals $l_m \approx 2\pi/V$, one obtains $x/l_m = xV/2\pi \ll 1$. Hence in this case the distance is very small and oscillation effect in the layer has double suppression.

3.10. Propagation in Multilayer Medium

3.10.1. Parametric Effects in the Neutrino Oscillations. The strong transitions discussed in the previous sections require the existence of large effective mixing, either in the entire medium (constant density) or at least in a layer (adiabatic conversion). There is a way to get strong transition without large vacuum or matter mixings. This can be realized with periodically or quasiperiodically changing density [24, 37] when the conditions of parametric resonance are satisfied. Although the flavor conversion in a layer which corresponds to one period is small, strong transitions can build up over several periods. For large mixing even a small number of periods are enough to obtain strong flavor transitions.

The usual condition of parametric resonance is that the period of density change T_n is an integer times the effective oscillation length l_m [38]:

$$\int_{l_T} \frac{dx}{l_m} = k, \quad (k = 1, 2, 3, \ldots), \tag{88}$$

or $l_T/\bar{l}_m = k$. Such an enhancement has been considered first for modulation of the profile by sine function [39]. This may have some applications for intense neutrino fluxes when neutrino-neutrino interactions become important.

The solvable case, which has simple physical interpretation, is provided by the *castle wall* profile, for which the period l_T is divided into the two parts l_1 and l_2 ($l_1 + l_2 = l_T$) with the densities n_1 and n_2, respectively ($n_1 \neq n_2$ and, in general, $l_1 \neq l_2$). Thus, the medium consists of alternating layers with two different densities [37, 40–45].

For the "castle wall" profile, the simplest realization of the parametric resonance condition is reduced to equality of the oscillation phases acquired by neutrinos over the two parts of the periods [41]:

$$\Phi_1 = \Phi_2 = \pi. \tag{89}$$

The enhancement of transition depends on the number of periods and on the amplitude of perturbation, which determines the swing angle (the difference of the mixing angles in the two layers, $\Delta\theta \equiv 2\theta_{1m} - 2\theta_{2m}$). For small $\Delta\theta$ a large transition probability can be achieved after many periods. For large "swing" angle, even a small number of periods are sufficient.

3.10.2. Parametric Enhancement: General Consideration. In general the condition (89) is not necessary for the enhancement or even for maximal enhancement. First, consider the oscillation effect over one period. The corresponding evolution matrix is given by the product

$$S_T = S_2 S_1, \tag{90}$$

where S_k ($k = 1, 2$) is the evolution in layer k given by (57). For brevity we will write it as $S_k = c_k I - i s_k (\sigma \cdot \mathbf{n}_k)$, $k = 1, 2$, where $c_k \equiv \cos\phi_k$, $s_k \equiv \sin\phi_k$, and ϕ_k is the half phase acquired in layer k:

$$\begin{aligned} \phi_k &= \frac{1}{2}\Delta H_k l_k = \frac{\Delta m^2}{4E} R (V_k)^{1/2} l_k, \\ \mathbf{n}_k &\equiv (\sin 2\theta_{mk}, 0, -\cos 2\theta_{mk}). \end{aligned} \tag{91}$$

Here θ_{mk} is the mixing angle in layer k.

Insertion of S_k from (57) into (90) gives [37]

$$S_T = Y\mathbf{I} - i(\sigma \cdot \mathbf{X}), \tag{92}$$

where

$$\begin{aligned} Y &\equiv c_1 c_2 - s_1 s_2 (\mathbf{n}_1 \cdot \mathbf{n}_2), \\ \mathbf{X} &= s_1 c_2 \mathbf{n}_1 + s_2 c_1 \mathbf{n}_2 - s_1 s_2 [\mathbf{n}_1 \times \mathbf{n}_2]. \end{aligned} \tag{93}$$

Explicitly, $(\mathbf{n}_1 \cdot \mathbf{n}_2) = \cos(2\theta_{m1} - 2\theta_{m2})$ and $[\mathbf{n}_1 \times \mathbf{n}_2] = \sin(2\theta_{m1} - 2\theta_{m2})\mathbf{e}_y$. Using unitarity of S_T, which gives $X^2 + Y^2 = 1$, one can parametrize X and Y with a new phase Φ as $Y \equiv \cos\Phi$ and $X \equiv \sin\Phi$. Then the evolution matrix S_T can be written in the form $S_T = \cos\Phi - i\sin\Phi(\sigma \cdot \widehat{\mathbf{X}}) = e^{-i(\sigma\cdot\widehat{\mathbf{X}})\Phi}$, where $\widehat{\mathbf{X}} \equiv \mathbf{X}/X$. Consequently, the evolution matrix after n periods equals

$$\begin{aligned} S^n &= (S_T)^n = e^{-i(\sigma\cdot\widehat{\mathbf{X}})n\Phi} \\ &= \cos n\Phi - i(\sigma \cdot \widehat{\mathbf{X}}) \sin n\Phi. \end{aligned} \tag{94}$$

It is simply accounted for by an increase of the phase: $\Phi \to n\Phi$. This is the consequence of the fact that the evolution matrices over all periods are equal and therefore commute. If the evolution ends at some instant t which does not coincide with the end of a full period, that is, $t = nT + t'$, then $S(t) = S(t')S_n$.

The transition probability computed with (94) is

$$P^n_{e\mu} = \left|S^n_{e\mu}\right|^2 = \frac{X_1^2 + X_2^2}{X^2}\sin^2 n\Phi. \tag{95}$$

It has the form of the usual oscillation probability with phase $n\Phi$ and depth $(X_1^2 + X_2^2)/X^2$. The oscillations described by (95) are called the parametric oscillations. Under condition

$$-X_3 = s_1c_2\cos 2\theta_{m1} + s_2c_1\cos 2\theta_{m2} = 0, \tag{96}$$

which is called the parametric resonance condition, the depth of oscillations (95) becomes 1 and the transition probability is maximal when $n\Phi = \pi/2 + \pi k$, where k is an integer. There are different realizations of the condition (96) which imply certain correlations among the mixing angles and phases. The simplest one, $c_1 = c_2 = 0$, coincides with (89).

3.10.3. Parametric Enhancement in Three Layers. For small number of layers an enhancement of flavor transition can occur due to certain relations between the phases and mixing angles in different layers. This in turn imposes certain conditions on the parameters of the layers: their densities and widths. The conditions are similar to the parametric resonance condition and this enhancement is called the *parametric enhancement* of flavor transitions. These conditions can be satisfied for certain energies and baselines for neutrinos propagating in the Earth.

Consider conditions for maximal enhancement of oscillations for a different number of layers. It is possible to show [46] that they are generalizations of the conditions in one layer which require that (i) the depth of oscillations is 1 (we call it the *amplitude condition*) and (ii) the oscillation phase is $\phi = \pi/2 + \pi k$—the *phase condition*.

Consider first the case of one layer with (in general) varying density (it can correspond to the mantle crossing trajectories in the Earth). The resonance condition for constant density case, $\cos 2\theta_m = 0$, can be written according to (22) and (51) as $\alpha = \alpha^*$, that is, $S^{(1)}_{11} = S^{(1)}_{22}$, or equivalently, $\mathrm{Im}\, S^{(1)}_{11} = 0$, where the superscript indicates the number of layers. This generalization goes beyond the original MSW resonance condition (even for constant density). The phase condition can be rewritten in terms of the elements of the evolution matrix (c.f., (54)) as $\mathrm{Re}\,\alpha \equiv \mathrm{Re}\, S^{(1)}_{11} = 0$. The absolute maximum of the transition probability occurs when these conditions are satisfied simultaneously, that is, when $S^{(1)}_{11} = 0$.

The parametric resonance condition (96) can be generalized to the case of nonconstant densities in the layers although the generalization is not unique. Indeed, according to (92) the condition $X_3 = 0$ can be written in terms of the elements of the evolution matrix for the two layers as the equality of the diagonal elements $S^{(2)}_{11} = S^{(2)}_{22}$. Let us find the conditions for extrema for density profiles consisting of two layers. We have $S^{(2)} = S_2S_1$, where $S^{(2)}_{11} = \alpha_2\alpha_1 - \beta_2\beta_1^*$, $S^{(2)}_{12} = \alpha_2\beta_1 + \beta_2\alpha_1^*$, and α_i, β_i for each layer have been defined in (51). The sum of the two complex numbers in the transition amplitude $S^{(2)}_{12}$ has the largest possible result if they have the same phase: $\arg(\alpha_2\beta_1) = \arg(\beta_2\alpha_1^*)$, which can also be rewritten as

$$\arg\left(\alpha_1\alpha_2\beta_1\right) = \arg\left(\beta_2\right). \tag{97}$$

This condition is called the *collinearity condition* [46]. It is an extremum condition for the two-layer transition probability under the constraint of fixed transition probabilities in the individual layers. In other words, if the absolute values $|\beta_i|$ of the transition amplitudes are fixed while their arguments are allowed to vary, then the transition probability reaches an extremum when these arguments satisfy (97).

The conditions for maximal transition probability for three layers can be found in the following way. The 1-2 elements of the evolution matrix $S^{(3)}$ equal

$$\begin{aligned} S^{(3)}_{12} &= \alpha_3S^{(2)}_{12} + \beta_3S^{(2)*}_{11} \\ &= \alpha_3\alpha_2\beta_1 + \alpha_3\beta_2\alpha_1^* + \beta_3\alpha_2^*\alpha_1^* - \beta_3\beta_2^*\beta_1. \end{aligned} \tag{98}$$

In the case of neutrino oscillations in the Earth, the third layer is just the second mantle layer, and its density profile is the reverse of that of the first layer. The evolution matrix for the third layer is therefore the transpose of that for the first one [47]; that is, $\alpha_3 = \alpha_1$, $\beta_3 = -\beta_1^*$, and the expression for $S^{(3)}_{12}$ can be written as

$$S^{(3)}_{12} = \alpha_1\alpha_2\beta_1 - \alpha_1^*\alpha_2^*\beta_1^* + \left|\alpha_1\right|^2\beta_2 + \left|\beta_1\right|^2\beta_2^*. \tag{99}$$

Note that β_2 is pure imaginary because the core density profile is symmetric. Therefore the amplitude $S^{(3)}_{12}$ in (99) is also pure imaginary, as it must be because the overall density profile of the Earth is symmetric as well. If the collinearity condition for two layers (97) is satisfied, then not only the full amplitude $S^{(3)}_{12}$, but also *each* of the four terms on the right-hand side of (99) is pure imaginary. If the collinearity condition is satisfied for two layers, then it is automatically satisfied for three layers. This is a consequence of the facts that the density profile of the third layer is the reverse of that of the first layer and that the second layer has a symmetric profile. The conditions described here allow reproducing very precisely all the main structures of the oscillograms of the Earth (see Section 4.1).

3.11. Oscillations of High Energy Neutrinos. At high energies or in high density medium when $V > \Delta m^2/2E$, we can use $\Delta/V \equiv \Delta m^2/4EV$ as a small parameter and develop a perturbation theory using its smallness. However, in most situations of interest, the neutrino path length in matter L is so large that $\Delta \cdot L \gtrsim 1$. Therefore the vacuum part of the Hamiltonian cannot be considered as a small perturbation in itself and the effect of Δ on the neutrino energy level splitting

should be taken into account. For this reason we split the Hamiltonian as $H = \widetilde{H}_0 + H_I$ with

$$\widetilde{H}_0 = \frac{\omega^m}{2}\begin{pmatrix}1 & 0\\ 0 & -1\end{pmatrix},$$
$$H_I = \sin 2\theta\Delta\begin{pmatrix}-\epsilon & 1\\ 1 & \epsilon\end{pmatrix}, \tag{100}$$

where ω^m is the oscillation frequency (20) and $\epsilon \equiv (2\Delta\cos 2\theta - V + \omega^m)/2\Delta\sin 2\theta \approx (\Delta/V)\sin 2\theta \ll 1$. The ratio of the second and the first terms in the Hamiltonian (100) is given by the mixing angle in matter θ_m: $2\Delta\sin 2\theta/\omega^m = \sin 2\theta_m$. Therefore for $\sin 2\theta_m \ll 1$ the term H_I can be considered as a perturbation. Furthermore, $\epsilon \sim \sin 2\theta_m$, so the diagonal terms in H_I can be neglected in the lowest approximation.

The solution for S matrix can be found in the form $S = S_0 \cdot S_I$, where S_0 is the solution of the evolution equation with H replaced by H_0 (see (71)). The matrix S_I then satisfies the equation

$$i\frac{dS_I}{dx} = S_0^{-1}H_I S_0 S_I = \widetilde{H}_I S_I, \tag{101}$$

where $\widetilde{H}_I \equiv S_0^{-1}H_I S_0$ is the perturbation Hamiltonian in the "interaction" representation. Equation (101) can be solved by iterations: $S_I = I + S_I^{(1)} + \ldots$, which leads to the standard perturbation series for the S matrix. For neutrino propagation between $x = 0$ and $x = L$ we have, to the lowest non-trivial order,

$$S(L) = S_0(L)\left[I - i\Delta\sin 2\theta\int_0^L dx\begin{pmatrix}0 & e^{i2\phi(x)}\\ e^{-i2\phi(x)} & 0\end{pmatrix}\right]. \tag{102}$$

The $\nu_e \leftrightarrow \nu_a$ transition probability $P_2 = [S(L)]_{ae}$ is given by

$$P_2 = \Delta^2\sin^2 2\theta\left|\int_0^L dx e^{-i2\phi(x)}\right|^2. \tag{103}$$

For density profiles that are symmetric with respect to the center of the neutrino trajectory, $V(x) = V(L-x)$, (103) gives

$$P_2 = 4\left(\frac{\Delta m^2}{4E}\right)^2\sin^2 2\theta\left[\int_0^{L/2} dz\cos 2\phi(z)\right]^2, \tag{104}$$

where $z = x - L/2$ is the distance from the midpoint of the trajectory and $\phi(z)$ is the phase acquired between this midpoint and the point z. The transition probability P_2 decreases with the increase of neutrino energy essentially as E^{-2}. The accuracy of (103) also improves with energy as E^{-2}.

Inside the Earth, the accuracy of the analytic formula is extremely good already for $E \gtrsim 8$ GeV. When neutrinos do not cross the Earth's core ($\cos\Theta > -0.837$) and so experience a slowly changing potential $V(x)$, the accuracy of the approximation (103) is very good even in the MSW resonance region $E \sim$ (5–8) GeV.

The above formalism applies in the low energy case as well, with only minor modifications: the sign of H_0 in (100) has to be flipped, and correspondingly one has to replace $\omega^m \to -\omega^m$ in the definition of ϵ. The expressions for the transition probability in (103) and (104) remain unchanged.

3.12. Effects of Small Density Perturbations. Let us consider perturbation around smooth profile for which exact solution is known. The simplest possibility that has implications for the Earth matter profile is the constant density with additional perturbation: $V(x) = \overline{V} + \Delta V(x)$. Correspondingly, the Hamiltonian of the system can be written as the sum of two terms:

$$H(x) = \overline{H} + \Delta H(x), \tag{105}$$

where

$$\overline{H} \equiv \overline{\omega}\begin{pmatrix}-\cos 2\overline{\theta} & \sin 2\overline{\theta}\\ \sin 2\overline{\theta} & \cos 2\overline{\theta}\end{pmatrix},$$
$$\Delta H \equiv \frac{\Delta V(x)}{2}\begin{pmatrix}1 & 0\\ 0 & -1\end{pmatrix}. \tag{106}$$

Here, $\overline{\theta} = \theta_m(\overline{V})$ is the mixing angle in matter and $\overline{\omega} = \omega^m(\overline{V})$ is half of the energy splitting (half-frequency) in matter, both with the average potential $\overline{V}$. We will denote by $\overline{S}(x)$ the evolution matrix of the system for the constant density case $H(x) = \overline{H}$. The expression for $\overline{S}(x)$ is given in (54) with $\theta_m = \overline{\theta}$ and $\phi_m(x) = \phi(x) \equiv \overline{\omega}x$, $\overline{\omega} = \omega^m(\overline{V})$.

The solution of the evolution equation with Hamiltonian (105) [46] is of the form

$$S(x) = \overline{S}(x) + \Delta S(x),$$
$$\Delta S(x) = -i\overline{S}(x)K_1(x), \tag{107}$$

where $K_1(x)$ satisfies $|K_1(x)_{ab}| \ll 1$. Inserting (107) into the evolution equation, one finds the following equation for $K_1(x)$ to the first order in $\Delta H(x)$ and $K_1(x)$:

$$\frac{dK_1(x)}{dx} = \overline{S}^\dagger\Delta H(x)\overline{S}$$
$$= \frac{\Delta V}{2}\left[-\cos 2\overline{\theta}\begin{pmatrix}-\cos 2\overline{\theta} & \sin 2\overline{\theta}\\ \sin 2\overline{\theta} & \cos 2\overline{\theta}\end{pmatrix}\right.$$
$$\left. + \sin 2\overline{\theta}\cos 2\phi\, G\left(\overline{\theta}\right) + \sin 2\overline{\theta}\sin 2\phi\sigma_2\right], \tag{108}$$

where $G(\overline{\theta}) \equiv \cos 2\overline{\theta}\sigma_1 + \sin 2\overline{\theta}\sigma_3$. The first term in (108) does not contribute to $S \equiv S(L)$ since $\langle\Delta V\rangle \equiv \int\Delta V(x)dx = 0$, and (108) can be immediately integrated:

$$K_1(L) = \frac{1}{2}\sin 2\overline{\theta}\left[G\left(\overline{\theta}\right)\int_0^L \Delta V(x)\cos 2\phi(x)\,dx\right.$$
$$\left. + \sigma_2\int_0^L \Delta V(x)\sin 2\phi(x)\,dx\right]. \tag{109}$$

Introducing the distance from the midpoint of the neutrino trajectory $z \equiv x - L/2$, one obtains from (109)

$$\Delta S \equiv \Delta S(L) = -i \sin 2\overline{\theta} \left[G\left(\overline{\theta}\right) \Delta I + \sigma_2 \Delta J \right], \tag{110}$$

where $\Delta I \equiv (1/2) \int_{-L/2}^{L/2} \Delta V(z) \cos(2\overline{\omega} z) dz$, $\Delta J \equiv (1/2) \int_{-L/2}^{L/2} \Delta V(z) \sin(2\overline{\omega} z) dz$. In these integrals, $\Delta V(z) \equiv \Delta V(x(z))$ and $x(z) = z - L/2$. The integral ΔJ vanishes if the perturbation $\Delta V(z)$ is symmetric with respect to the midpoint of the trajectory. Analogously, ΔI vanishes if $\Delta V(z)$ is antisymmetric. The expression for S defined in (107) is equivalent to (13)–(16) obtained in [48] in the context of solar neutrino oscillations.

For practical purposes it is useful to have an expression for S which is *exactly* unitary regardless of the size of the perturbation. For this we rewrite (110) as follows:

$$\begin{aligned} \Delta S &= \varepsilon S', \\ S' &= -i \left[G\left(\overline{\theta}\right) \cos\xi + \sigma_2 \sin\xi \right], \end{aligned} \tag{111}$$

where $\sin\xi = \Delta J / \sqrt{(\Delta J)^2 + (\Delta I)^2}$ and $\epsilon = \sin 2\overline{\theta} \cdot \sqrt{(\Delta J)^2 + (\Delta I)^2}$. Thus, $S = \overline{S} + \varepsilon S'$ and we replace it by

$$S = \cos\varepsilon \overline{S} + \sin\varepsilon S'. \tag{112}$$

Here both S' and $\overline{S}$ are unitary matrices, and due to their specific form the combination on the right-hand side of (112) is exactly unitary.

For a symmetric density profile with respect to the midpoint of the trajectory, the term ΔJ is absent. From (54), (110), and (112) we immediately get the transition probability

$$\begin{aligned} P &= \left[\cos\varepsilon \sin 2\overline{\theta} \sin\phi + \sin\varepsilon \cos 2\overline{\theta} \right]^2 \\ &\approx \sin^2 2\overline{\theta} \left[\sin\phi + \Delta I \cos 2\overline{\theta} \right]^2, \end{aligned} \tag{113}$$

where $\varepsilon \equiv \sin 2\overline{\theta}\ \Delta I$ and $\phi \equiv \phi(L) = \overline{\omega} L$. Here the first term in the square brackets describes oscillations in constant density matter with average potential $\overline{V}_1$.

3.13. Oscillation Probabilities and Their Properties. It is convenient to consider the neutrino flavor evolution in the propagation basis $\widetilde{\nu} = (\nu_e, \widetilde{\nu}_2, \widetilde{\nu}_3)^T$, defined in (27). In this basis propagation is not affected by the 2-3 mixing and CP violation. The dependence on these parameters appears when one projects the initial flavor state on the propagation basis and the final state back onto the original flavor basis. The propagation-basis states are related to the mass states as

$$\widetilde{\nu} = U_{13} I_{-\delta} U_{12} \nu. \tag{114}$$

Since the transformations, which connect $\widetilde{\nu}$ and ν_f, do not depend on matter potential and therefore distance, the states $\widetilde{\nu}$ satisfy the evolution equation $i(d\widetilde{\nu}/dt) = \widetilde{H}\widetilde{\nu}$, with the Hamiltonian $\widetilde{H}$ defined in (28).

3.13.1. S Matrix and Oscillation Amplitudes. A number of properties of the oscillation probabilities can be obtained from general consideration of matrix of the oscillation amplitudes. We introduce the evolution matrix (the matrix of amplitudes) in the propagation basis as

$$\widetilde{S} = \begin{pmatrix} A_{ee} & A_{e\widetilde{2}} & A_{e\widetilde{3}} \\ A_{\widetilde{2}e} & A_{\widetilde{2}\widetilde{2}} & A_{\widetilde{2}\widetilde{3}} \\ A_{\widetilde{3}e} & A_{\widetilde{3}\widetilde{2}} & A_{\widetilde{3}\widetilde{3}} \end{pmatrix}. \tag{115}$$

Then according to (27) the S matrix in the flavor basis equals

$$\begin{aligned} S &= \widetilde{U}\widetilde{S}\widetilde{U}^{\dagger}, \\ \widetilde{U} &\equiv U_{23} I_{\delta}. \end{aligned} \tag{116}$$

In this part, we use the notation A_{ij} for the amplitudes in the propagation basis and S_{ij} for the amplitudes in the flavor basis. In terms of the propagation-basis amplitudes (115) the S matrix in the flavor basis can be written as

$$S = \begin{pmatrix} A_{ee} & c_{23}A_{e\widetilde{2}} + s_{23}e^{-i\delta}A_{e\widetilde{3}} & -s_{23}A_{e\widetilde{2}} + c_{23}e^{-i\delta}A_{e\widetilde{3}} \\ c_{23}A_{\widetilde{2}e} + s_{23}e^{i\delta}A_{\widetilde{3}e} & c_{23}^2 A_{\widetilde{2}\widetilde{2}} + s_{23}^2 A_{\widetilde{3}\widetilde{3}} + K_{\mu\mu} & -s_{23}c_{23}\left(A_{\widetilde{2}\widetilde{2}} - A_{\widetilde{3}\widetilde{3}}\right) + K_{\mu\tau} \\ -s_{23}A_{\widetilde{2}e} + c_{23}e^{i\delta}A_{\widetilde{3}e} & -s_{23}c_{23}\left(A_{\widetilde{2}\widetilde{2}} - A_{\widetilde{3}\widetilde{3}}\right) + K_{\tau\mu} & s_{23}^2 A_{\widetilde{2}\widetilde{2}} + c_{23}^2 A_{\widetilde{3}\widetilde{3}} + K_{\tau\tau} \end{pmatrix}, \tag{117}$$

where

$$\begin{aligned} K_{\mu\mu} &\equiv s_{23}c_{23}\left(e^{-i\delta}A_{\widetilde{2}\widetilde{3}} + e^{i\delta}A_{\widetilde{3}\widetilde{2}}\right), \\ K_{\mu\tau} &\equiv c_{23}^2 e^{-i\delta}A_{\widetilde{2}\widetilde{3}} - s_{23}^2 e^{i\delta}A_{\widetilde{3}\widetilde{2}}, \\ K_{\tau\mu} &= K_{\mu\tau}\left(\delta \longrightarrow -\delta, \widetilde{2} \longleftrightarrow \widetilde{3}\right), \\ K_{\tau\tau} &= -K_{\mu\mu}. \end{aligned} \tag{118}$$

The scheme of transitions is shown in Figure 7. There is certain hierarchy of the amplitudes which can be obtained immediately from the form of the Hamiltonian in the propagation basis (29):

$$\begin{aligned} &A_{e\widetilde{3}}, A_{\widetilde{3}e} \sim s_{13}, \\ &A_{e\widetilde{2}}, A_{\widetilde{2}e} \sim r_{\Delta} \sim s_{13}^2, \\ &A_{\widetilde{3}\widetilde{2}}, A_{\widetilde{2}\widetilde{3}} \sim s_{13} r_{\Delta} \sim s_{13}^3, \end{aligned} \tag{119}$$

that is, $A_{\widetilde{2}\widetilde{3}}$ and $A_{\widetilde{3}\widetilde{2}}$ are the smallest amplitudes. In the propagation basis there is no fundamental CP or T violation. Therefore for a symmetric density profile with respect to the middle point of trajectory (as in the case of the Earth) the neutrino evolution is T invariant which yields

$$\begin{aligned} A_{\widetilde{2}e} &= A_{e\widetilde{2}}, \\ A_{\widetilde{3}e} &= A_{e\widetilde{3}}, \\ A_{\widetilde{3}\widetilde{2}} &= A_{\widetilde{2}\widetilde{3}}. \end{aligned} \tag{120}$$

Consequently, for $K_{\alpha\beta}$ we obtain

$$\begin{aligned} K_{\mu\tau} &= A_{\widetilde{2}\widetilde{3}}\left(\cos 2\theta_{23}\cos\delta - i\sin\delta\right), \\ K_{\tau\mu} &= K_{\mu\tau}\left(\delta \longrightarrow -\delta\right), \\ K_{\mu\mu} &= -K_{\tau\tau} = A_{\widetilde{2}\widetilde{3}}\sin 2\theta_{23}\cos\delta. \end{aligned} \tag{121}$$

These terms proportional to small amplitudes $A_{\widetilde{2}\widetilde{3}}$ and $A_{\widetilde{3}\widetilde{2}}$ are of the order $O(s_{13}^2)$.

For a symmetric density profile, from (117), (120), and (121) one finds for the probabilities $P_{\alpha\beta} \equiv |S_{\beta\alpha}|^2$:

$$P_{ee} = \left|A_{ee}\right|^2 = 1 - \left|A_{e\widetilde{2}}\right|^2 - \left|A_{e\widetilde{3}}\right|^2, \tag{122}$$

$$\begin{aligned} P_{\mu e} = {} & c_{23}^2\left|A_{e\widetilde{2}}\right|^2 + s_{23}^2\left|A_{e\widetilde{3}}\right|^2 \\ & + 2s_{23}c_{23}\,\mathrm{Re}\left(e^{-i\delta}A_{e\widetilde{2}}^{*}A_{e\widetilde{3}}\right), \end{aligned} \tag{123}$$

$$\begin{aligned} P_{\tau e} = {} & s_{23}^2\left|A_{e\widetilde{2}}\right|^2 + c_{23}^2\left|A_{e\widetilde{3}}\right|^2 \\ & - 2s_{23}c_{23}\,\mathrm{Re}\left(e^{-i\delta}A_{e\widetilde{2}}^{*}A_{e\widetilde{3}}\right), \end{aligned} \tag{124}$$

$$\begin{aligned} P_{\mu\mu} = {} & \left|c_{23}^2A_{\widetilde{2}\widetilde{2}} + s_{23}^2A_{\widetilde{3}\widetilde{3}}\right. \\ & \left. +2s_{23}c_{23}\cos\delta A_{\widetilde{2}\widetilde{3}}\right|^2, \end{aligned} \tag{125}$$

$$\begin{aligned} P_{\mu\tau} = {} & \left|s_{23}c_{23}\left(A_{\widetilde{3}\widetilde{3}} - A_{\widetilde{2}\widetilde{2}}\right)\right. \\ & \left. + \left(\cos 2\theta_{23}\cos\delta + i\sin\delta\right)A_{\widetilde{2}\widetilde{3}}\right|^2. \end{aligned} \tag{126}$$

For antineutrinos the amplitudes can be obtained from the results presented above substituting

$$\begin{aligned} &\delta \longrightarrow -\delta, \qquad A_{ij} \longrightarrow \overline{A}_{ij}, \\ &\text{where } \overline{A}_{ij} \equiv A_{ij}\left(V \longrightarrow -V\right). \end{aligned} \tag{127}$$

Notice that the amplitudes of transitions (123) and (124), that involve ν_e, are given by linear combinations of two propagation-basis amplitudes. The other flavor amplitudes depend on three propagation-basis amplitudes.

3.13.2. Factorization Approximation and Amplitudes for Constant Density. As follows immediately from the form of the Hamiltonian $\widetilde{H}$ in (29), in the limits $\Delta m_{21}^2 \to 0$ or/and $s_{12} \to 0$ the state $\widetilde{\nu}_2$ decouples from the rest of the system, and consequently, the amplitude $A_{e\widetilde{2}}$ vanishes. In this limit, $A_{e\widetilde{3}}$ (as well as $A_{\widetilde{3}\widetilde{3}}$ and S_{ee}) is reduced to a 2ν amplitude which depends on the parameters Δm_{31}^2 and θ_{13}: $A_A(\Delta m_{31}^2, \theta_{13}) \equiv A_{e\widetilde{3}}(\Delta m_{21}^2 = 0)$. The corresponding probability equals $P_A \equiv |A_A|^2$.

In the limit $s_{13} \to 0$ the state $\widetilde{\nu}_3$ decouples while the amplitude $A_{e\widetilde{3}}$ vanishes and the amplitude $A_{e\widetilde{2}}$ reduces to a 2ν amplitude depending on the parameters of the 1-2 sector, Δm_{21}^2 and θ_{12}. Denoting this amplitude by A_S we have $A_S(\Delta m_{21}^2, \theta_{12}) \equiv A_{e\widetilde{2}}(\theta_{13} = 0)$. We will use the notation $P_S \equiv |A_S|^2$.

This consideration implies that to the leading nontrivial order in the small parameters s_{13} and r_Δ the amplitudes $A_{e\widetilde{2}}$ and $A_{\widetilde{2}e}$ are reduced to two neutrino probabilities and depend only on the "solar" parameters, whereas the amplitudes $A_{e\widetilde{3}}$ and $A_{\widetilde{3}e}$ only on the "atmospheric" parameters:

$$\begin{aligned} A_{e\widetilde{2}} &\simeq A_{\widetilde{2}e} \simeq A_S\left(\Delta m_{21}^2, \theta_{12}\right), \\ A_{e\widetilde{3}} &\simeq A_{\widetilde{3}e} \simeq A_A\left(\Delta m_{31}^2, \theta_{13}\right). \end{aligned} \tag{128}$$

The approximate equalities in (128) are called the factorization approximation.

Due to the level crossing phenomenon the factorization approximation (128) is not valid in the energy range of the 1–3 resonance where the 1–3 mixing in matter is enhanced. In the case of a matter with an arbitrary density profile, one can show, using simple power counting arguments, that the corrections to the factorization approximation for the amplitude $A_{e\widetilde{2}}$ are of order s_{13}^2, whereas the corrections to the "atmospheric" amplitude $A_{e\widetilde{3}}$ are of order r_Δ [49], in agreement with our consideration for constant density. The amplitude $A_{e\widetilde{3}}$ does not in general have a 2-flavor form, once the corrections to the factorization approximation are taken into account.

Using the expressions for U_{ei}^m and $U_{\mu i}^m$ in terms of the mixing angles in the standard parametrization, we can rewrite (67) as

$$S_{e\mu}^{\mathrm{cst}} = \cos\theta_{23}^m A_{e\widetilde{2}}^{\mathrm{cst}} + \sin\theta_{23}^m e^{-i\delta^m} A_{e\widetilde{3}}^{\mathrm{cst}}, \tag{129}$$

where

$$\begin{aligned} A_{e\widetilde{2}}^{\mathrm{cst}} &\equiv -ie^{i\phi_{21}^m}\cos\theta_{13}^m\sin 2\theta_{12}^m\sin\phi_{21}^m, \\ A_{e\widetilde{3}}^{\mathrm{cst}} &\equiv -ie^{i\phi_{21}^m}\sin 2\theta_{13}^m\left[\sin\phi_{32}^m\; e^{-i\phi_{31}^m} + \cos^2\theta_{12}^m\sin\phi_{21}^m\right]. \end{aligned} \tag{130}$$

Here $\phi_{31}^m = \phi_{32}^m + \phi_{21}^m$. Since to a good approximation $\theta_{23}^m \approx \theta_{23}$ and $\delta^m \approx \delta$ (see Section 2.5) [20, 50], the amplitudes $A_{e\widetilde{2}}^{\mathrm{cst}}$ and $A_{e\widetilde{3}}^{\mathrm{cst}}$ can be identified with $A_{e\widetilde{2}}$ and $A_{e\widetilde{3}}$ in (123) and (124).

In terms of mixing angles, $U_{\mu 1}^m = -s_{12}^m c_{23}^m - c_{12}^m s_{13}^m s_{23}^m e^{i\delta^m}$, $U_{\mu 3}^m = c_{13}^m s_{23}^m$, the amplitude $S_{\mu\mu}^{\mathrm{cst}}$ can be rewritten as

$$\begin{aligned} S_{\mu\mu}^{\mathrm{cst}} = {} & \cos^2\theta_{23}^m A_{\widetilde{2}\widetilde{2}}^{\mathrm{cst}} \\ & + \sin^2\theta_{23}^m A_{\widetilde{3}\widetilde{3}}^{\mathrm{cst}} + \sin 2\theta_{23}^m\cos\delta^m A_{\widetilde{2}\widetilde{3}}^{\mathrm{cst}}, \end{aligned} \tag{131}$$

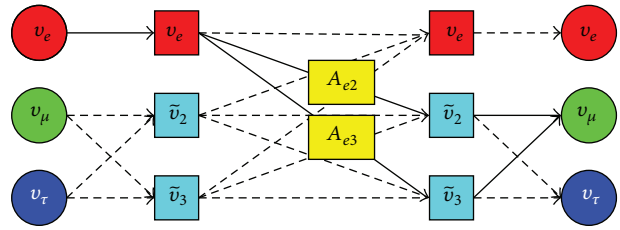

Figure 7: Scheme of transitions between the flavor states. Evolution is considered in the propagation basis $\tilde{\nu}$. The lines which connect the flavor states and the propagation-basis states indicated projection of one basis onto another. The lines connecting the states of propagation basis $\tilde{\nu}$ show transitions between them.

where

$$\begin{aligned} A^{\mathrm{cst}}_{\tilde{2}\tilde{2}} &\equiv 1 + 2ie^{i\phi^m_{21}} \sin^2\theta^m_{12} \sin\phi^m_{21}, \\ A^{\mathrm{cst}}_{\tilde{3}\tilde{3}} &\equiv 1 - 2ie^{-i\phi^m_{32}} \cos^2\theta^m_{13} \sin\phi^m_{32} \\ &\quad + 2ie^{i\phi^m_{21}} \sin^2\theta^m_{13} \cos^2\theta^m_{12} \sin\phi^m_{21}, \\ A^{\mathrm{cst}}_{\tilde{2}\tilde{3}} &\equiv ie^{i\phi^m_{21}} \sin\theta^m_{13} \sin 2\theta^m_{12} \sin\phi^m_{21}. \end{aligned} \tag{132}$$

Notice that $A^{\mathrm{cst}}_{\tilde{2}\tilde{2}}$ has exactly the form of the corresponding 2ν amplitude driven by the solar parameters. The amplitude $A^{\mathrm{cst}}_{\tilde{3}\tilde{3}}$ also coincides to a very good approximation with the corresponding 2ν amplitude driven by the atmospheric parameters. In the approximation $\theta^m_{23} \approx \theta_{23}$ and $\delta^m \approx \delta$ the amplitudes (132) can be identified with the corresponding amplitudes in the propagation basis.

3.13.3. Properties of the Flavor Oscillation Probabilities

(1) ν_e-ν_e channel: the total probability of the ν_e disappearance equals

$$1 - P_{ee} = P_{e\mu} + P_{e\tau} = P_{e\tilde{2}} + P_{e\tilde{3}}. \tag{133}$$

The probability P_{ee} does not depend on the CP-violating phase and the 2-3 mixing in the standard parametrization. The interference of the solar and atmospheric modes in P_{ee} originates mainly from $P_{e\tilde{3}} \equiv |A_{e\tilde{3}}|^2$. The survival probability then equals $P_{ee} = 1 - P_{e\mu} - P_{e\tau} = 1 - P_A - P_S$. At high energies, where the effects of the 1-2 mixing and mass splitting in P are suppressed, the probability is $P_{ee} \approx 1 - P_{e\tau} \approx 1 - P_A$.

(2) ν_e-ν_μ and ν_e-ν_τ channels: the transition probability $P_{\mu e} \equiv P(\nu_\mu \to \nu_e)$ (see (123)) can be rewritten as

$$\begin{aligned} P_{\mu e} &= c^2_{23}\left|A_{e\tilde{2}}\right|^2 + s^2_{23}\left|A_{e\tilde{3}}\right|^2 \\ &\quad + \sin 2\theta_{23}\left|A^*_{e\tilde{2}}A_{e\tilde{3}}\right| \cos\left(\phi - \delta\right), \end{aligned} \tag{134}$$

where $\phi \equiv \arg(A^*_{e\tilde{2}}A_{e\tilde{3}})$. Unlike $1-P_{ee}$, this probability contains the interference term between $A_{e\tilde{2}}$ and $A_{e\tilde{3}}$ which depends on the CP violation phase. Since the amplitude $A_{e\tilde{2}}$ is suppressed at high energies due to the smallness of the 1-2 mixing in matter, in the lowest approximation we have

$$P_{\mu e} \approx \sin^2\theta_{23}\left|A_{e\tilde{3}}\right|^2 \approx \sin^2\theta_{23}\left|A_A\right|^2. \tag{135}$$

The maximal value of the probability equals $P_{\mu e} \simeq s^2_{23}$. According to (123) and (124) the oscillation probabilities $P_{\tau e}$ and $P_{e\tau}$ can be obtained from the corresponding probabilities $P_{\mu e}$ and $P_{e\mu}$ through the substitution $s_{23} \to c_{23}$, $c_{23} \to -s_{23}$ [51]. The interference term has the opposite signs for channels including ν_τ as compared with those with ν_μ, which can be obtained from the unitarity condition $P_{ee} + P_{\mu e} + P_{\tau e} = 1$ and the fact that P_{ee} does not depend on δ.

(3) The ν_μ survival probability, $P_{\mu\mu}$, for symmetric density profiles, (125), can be rewritten as

$$\begin{aligned} P_{\mu\mu} &= \left|c^2_{23}A_{\tilde{2}\tilde{2}} + s^2_{23}A_{\tilde{3}\tilde{3}}\right|^2 \\ &\quad + 2\sin 2\theta_{23}\cos\delta\ \mathrm{Re}\left[A^*_{\tilde{2}\tilde{3}}\left(c^2_{23}A_{\tilde{2}\tilde{2}} + s^2_{23}A_{\tilde{3}\tilde{3}}\right)\right] \\ &\quad + \sin^2 2\theta_{23}\cos^2\delta\left|A_{\tilde{2}\tilde{3}}\right|^2. \end{aligned} \tag{136}$$

Since $A_{\tilde{2}\tilde{3}} = \mathcal{O}(r_\Delta s_{13})$ is a small quantity, to a good approximation one can neglect the term $\sim \cos^2\delta$ in (125), which is proportional to $|A_{\tilde{2}\tilde{3}}|^2$. For high energies in the limit $\Delta m^2_{21} \to 0$ we have $A_{\tilde{2}\tilde{2}} = 1$, $A_{\tilde{2}\tilde{3}} = 0$. Then, parameterizing the 33-amplitude as $A_{\tilde{3}\tilde{3}} = \sqrt{1-P_A}e^{-i\phi^m_{\tilde{3}\tilde{3}}}$ we obtain from (136)

$$\begin{aligned} &P_{\mu\mu}\left(\Delta m^2_{21} = 0\right) \\ &\quad = 1 - \sin^2 2\theta_{23}\sin^2\phi_x - s^4_{23}P_A \\ &\quad\quad - 0.5\sin^2 2\theta_{23}\cos 2\phi_X\left(1 - \sqrt{1-P_A}\right), \end{aligned} \tag{137}$$

where $\phi_X = 0.5\arg[A^*_{\tilde{3}\tilde{3}}A_{\tilde{2}\tilde{2}}] = \phi^m_{\tilde{2}\tilde{2}} - \phi^m_{\tilde{3}\tilde{3}}$. The probability can be rewritten as

$$\begin{aligned} P_{\mu\mu} &= 1 - 0.5\sin^2 2\theta_{23} - s^4_{23}P_A \\ &\quad + 0.5\sin^2 2\theta_{23}\left(\sqrt{1-P_A}\right)\cos 2\phi_X. \end{aligned} \tag{138}$$

(4) ν_μ-ν_τ channel: for symmetric matter density profiles the probability of $\nu_\mu \to \nu_\tau$ oscillations is given in (126). It can be rewritten as

$$\begin{aligned} P_{\mu\tau} = {} & \frac{1}{4}\sin^2 2\theta_{23}\left|A_{\widetilde{2}\widetilde{2}} - A_{\widetilde{3}\widetilde{3}}\right|^2 \\ & + \sin 2\theta_{23}\cos 2\theta_{23}\cos\delta\ \mathrm{Re}\left[\left(A^*_{\widetilde{3}\widetilde{3}} - A^*_{\widetilde{2}\widetilde{2}}\right)A_{\widetilde{2}\widetilde{3}}\right] \\ & - \sin 2\theta_{23}\sin\delta\ \mathrm{Im}\left[A^*_{e\widetilde{2}}A_{e\widetilde{3}}\right] \\ & + \left(1 - \sin^2 2\theta_{23}\cos^2\delta\right)\left|A_{\widetilde{2}\widetilde{3}}\right|^2. \end{aligned} \tag{139}$$

The amplitude depends on δ through the terms proportional to $\cos\delta$ and $\sin\delta$, and therefore $P_{\mu\tau}$ contains both CP- and T-even and -odd terms. One can show that the δ-dependent interference terms, which are proportional to $\sin\delta$ and $\cos\delta$, satisfy the relation $P^\delta_{\mu\tau} = -P^\delta_{\mu e} - P^\delta_{\mu\mu}$. In the limit $\Delta m^2_{21} \to 0$ we obtain

$$\begin{aligned} P_{\mu\tau} = {} & 0.5\sin^2 2\theta_{23} - s^2_{23}c^2_{23}P_A \\ & - 0.5\sin^2 2\theta_{23}\left(\sqrt{1 - P_A}\right)\cos 2\phi_X. \end{aligned} \tag{140}$$

4. Matter Effects and Determination of Neutrino Mass Hierarchy

4.1. Propagation of Neutrinos through the Earth. Flavor neutrino evolution in the Earth is essentially oscillations in a multi-layer medium with slowly changing density in the individual layers and sharp density change on the borders of layers. For energies $E > 0.1$ GeV, possible short-scale inhomogeneities of the matter distribution can be neglected and the density profile experienced by neutrinos is symmetric with respect to the midpoint of the trajectory:

$$V(x) = V(L - x). \tag{141}$$

Here $L = 2R_\oplus|\cos\theta_z|$ is the length of the trajectory inside the Earth, $R_\oplus = 6371$ km is the Earth radius, and θ_z is the zenith angle related to the nadir angle as $\Theta_\nu = \pi - \theta_z$. For $0 \le \Theta_\nu \le 33.1^\circ$ neutrinos cross both the mantle and the core of the Earth, whereas for larger values of the nadir angle they only cross the Earth's mantle. The column density of the Earth along the diameter equals $d_{\mathrm{Earth}} = \int n(x)dx$, which is bigger than the minimal width; the size of the Earth is comparable with the neutrino refraction length.

For the 1-2 channel, the adiabaticity is well satisfied for all energies. We can therefore use the adiabatic approximation. The results of the evolution are determined by the mixing at the surface of the Earth and by the adiabatic phase. In the 1–3 channel the adiabaticity is broken at the resonance. Thus, the constant density approximation with the average density works well in this regime. For energies below the resonance the matter effect becomes small and the constant density approximation and the adiabatic approximation give very similar results.

For the core-crossing trajectories, the profile consists of three layers in the first approximation: (i) mantle (with increasing density), (ii) core (with a symmetric profile), and (iii) second mantle layer (with decreasing density). This second mantle layer is T-inverted with respect to the first. In this approximation the profile can be considered as three layers of constant effective densities. As such, it looks like a part (1.5 period) of the castle wall profile. Consequently, the parametric enhancement of oscillations, and in particular, the parametric resonance can be realized.

4.1.1. Neutrino Oscillograms of the Earth. A comprehensive description of effects of neutrino passage through the Earth can be obtained in terms of neutrino oscillograms. The oscillograms are defined as lines of equal probabilities (or certain combinations of probabilities) in the E_ν-$\cos\theta_z$ plane. In Figure 8, we show the oscillograms for the oscillation probabilities $P_{e\mu}$ and $P_{\mu\mu}$, as well as the corresponding probabilities for antineutrinos [43, 46, 52–55].

The structure of the oscillograms is well defined and unique and reflects the structure of the Earth as well as the properties of the neutrinos themselves. In a sense, the oscillograms are the neutrino images of the Earth. In contrast to usual light, there are several different images in different flavors as well as in neutrinos and antineutrinos.

The positions of all main structures of the oscillograms are determined by different realizations of the amplitude condition and the phase condition. These are generalizations of the condition for maximal flavor transitions in the case of vacuum oscillations or oscillation in uniform matter. Recall that, in the latter case, $P = 1$ requires

(i) $\sin^2 2\theta_m = 1$, the amplitude condition, which is nothing but the MSW resonance condition, and

(ii) $\phi = \pi/2 + \pi k$, the phase condition.

At $E > 1$ GeV the main structures of oscillograms are generated by the 1–3 mixing. They include the following.

(1) The MSW resonance pattern (resonance enhancement of the oscillations) for trajectories crossing only the mantle, with the main peak at $E_\nu \sim$ (5–7) GeV. The position of the maximum is given by the MSW resonance condition:

$$E_\nu = E_R(\Theta_\nu) = \frac{\Delta m^2_{31}\cos 2\theta_{13}}{2\overline{V}_1(\Theta_\nu)}, \tag{142}$$

where $\overline{V}_1(\Theta_\nu)$ is the average value of the potential along the trajectory characterized by Θ_ν. The phase condition becomes $2\phi(E_\nu, \Theta_\nu) = 2\omega(\overline{V}, E_\nu)L(\Theta_\nu) = \pi$ and the intersection of the resonance and the phase condition lines gives the absolute maximum of P_A. Combining these conditions gives the coordinates of the peak: $\cos\Theta_\nu = 0.77$ and $E_R = 6$ GeV.

(2) Three parametric ridges in the domain of core-crossing trajectories $|\cos\theta_z| > 0.87$ and $E_\nu > 3$ GeV. The parametric ridges differ by the oscillation phase acquired in the core, ϕ_2.

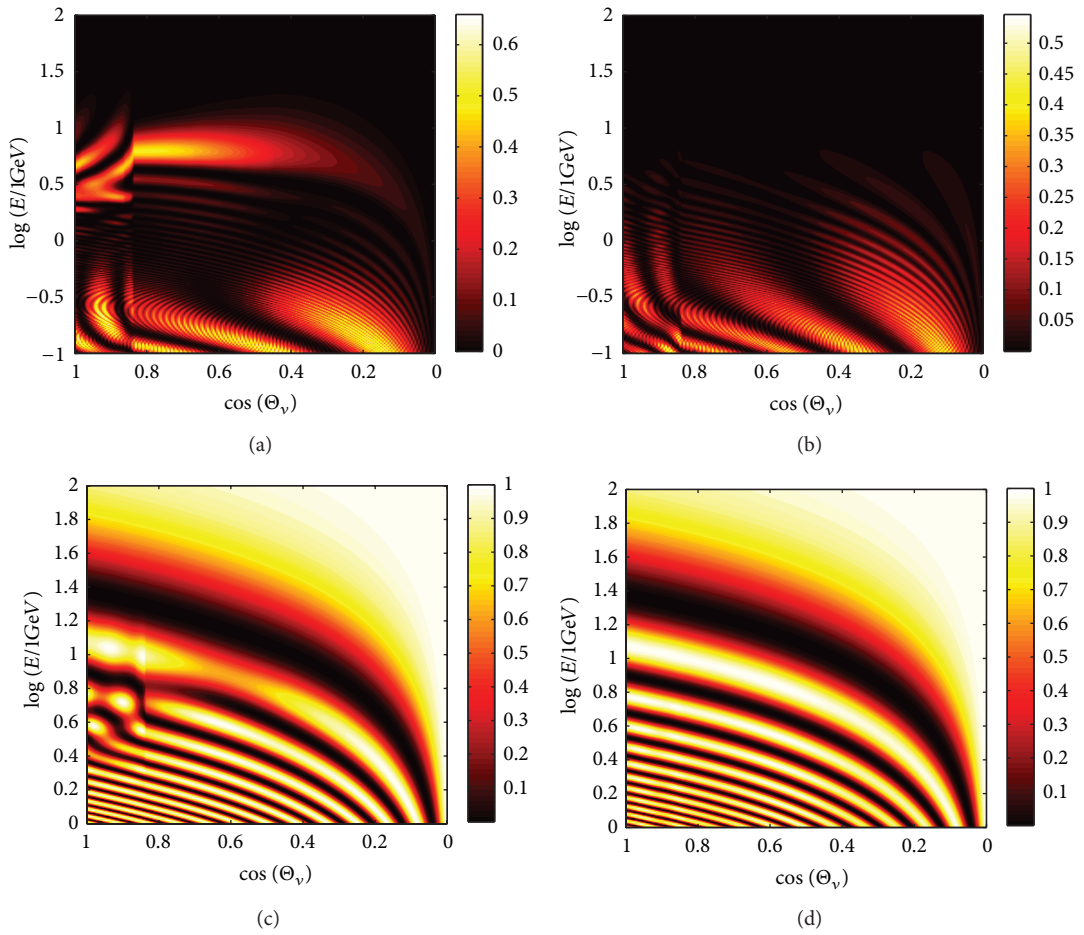

FIGURE 8: Neutrino oscillograms of the Earth. Shown are the lines of equal flavor conversion probability in the E_ν-cosΘ_ν plane. Upper panels: $\nu_e \to \nu_\mu$ (left) and $\bar{\nu}_e \to \bar{\nu}_\mu$ (right); bottom panels: $\nu_\mu \to \nu_\mu$ (left) and $\bar{\nu}_\mu \to \bar{\nu}_\mu$ (right). Normal hierarchy is assumed.

(i) *Ridge A* lies between the core resonance (at $\Theta_\nu \sim 0^\circ$) and the mantle resonance regions, $E_\nu \approx 3$–6 GeV. The phase in the core is $\phi_2 \lesssim \pi$. This ridge merges with the MSW resonance peak in the mantle.

(ii) *Ridge B* is situated at $E_\nu \geq 5$ GeV. For the lowest energies in the ridge and $\Theta_\nu \sim 0$, the half phase in the core equals $\phi_2 \sim (1.2\text{-}1.3)\pi$.

(iii) *Ridge C* is located at $E_\nu > 11$ GeV in the matter dominated region, where the mixing and, consequently, oscillation depth are suppressed.

(3) The MSW resonance peak in core located at $E_\nu \sim$ 2.5–2.8 GeV.

(4) The regular oscillatory pattern at low energies with "valleys" of zero probability and ridges in the mantle domain and a more complicated pattern with local maxima and saddle points in the core domain.

In Figure 9, we show graphic representations of oscillations which correspond to salient features of the oscillograms.

For energies $E_\nu < 1$ GeV the main structures are induced by the 1-2 mixing with small corrections due to 1–3 vacuum oscillations. Neglecting effect of θ_{13} we have $1 - P_{ee} = |A_{e\tilde{2}}|^2 \equiv P_S$. The probabilities of the modes including ν_e are expressed in terms of a unique probability P_S.

The 1-2 pattern differs from the pattern for the 1–3 mixing due to the large value of the 1-2 mixing. The oscillation length at the resonance is smaller than that for the 1–3 mixing, $l_m^R = l_\nu / \sin 2\theta_{12} \sim l_\nu$. The resonance energy is shifted to smaller values both due to $\Delta m^2_{21} \ll \Delta m^2_{31}$ and because of the factor $\cos 2\theta_{12} \approx 0.4$: $E_{12}^R = (\Delta m^2_{21}/2\overline{V}) \cos 2\theta_{12}$. Here $\overline{V}$ is the average value of the potential. The adiabaticity is better satisfied than for the 1–3 mixing case and therefore the oscillation probability in the mantle is determined by the potential near the surface of the Earth $\overline{V}$ averaged over a distance of the order of the first oscillation length. The oscillation length in matter l_m monotonically increases with energy, approaching the refraction length $l_0 \equiv 2\pi/V$ (c.f. Figure 4). The jump of the mixing angle at the mantle-core boundary is small. Thus, the sudden distortion of the oscillation patterns at $\Theta_\nu = 33^\circ$ is not as significant as it is for the 1–3 mixing, in particular below the 1-2 resonance energy. These features allow understanding the structure of the oscillograms. In the mantle domain ($\Theta_\nu > 33^\circ$)

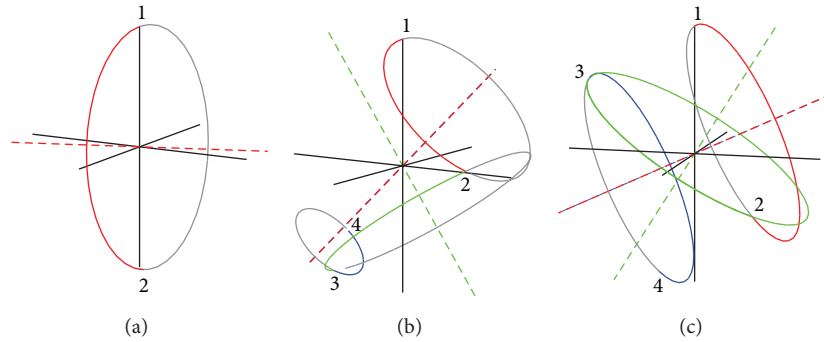

Figure 9: Graphic representation of transition in different points of oscillogram: peak due to MSW resonance in the mantle (left), peak due to parametric enhancement of transition driven by 1–3 mixing (middle), and peak due to parametric enhancement of transition driven by 1-2 mixing (right). In the left panel, neutrinos traverse only the mantle layer. In the right panel, neutrinos traverse the mantle (red), the core (green), and again the mantle (blue). The dashed lines correspond to the Hamiltonian vector **H** for the mantle (red) and core (green), respectively.

the oscillation pattern for neutrinos is determined by the resonance enhancement of oscillations. There are three MSW resonance peaks above 0.1 GeV, which differ from each other by value of the total oscillation phase. The outer peak ($\Theta_\nu \approx 82^\circ$) corresponds to $\phi \approx \pi/2$, the middle ($\Theta_\nu = 60^\circ$) to $\phi \approx 3\pi/2$, and the inner ($\Theta_\nu \approx 40^\circ$) to $\phi = 5\pi/2$. Recall that such a large phase can be acquired due to the smaller resonance oscillation length in comparison to that of the 1–3 mixing case, for which only one peak with $\phi = \pi/2$ can be realized. The resonance energy is given by (45), and for the surface potential we find

$$E_{12}^R \approx 0.12\,\text{GeV}. \tag{143}$$

The ratio of the 1-2 and 1–3 resonance energies equals $E_{12}^R/E_{13}^R \approx 1/50$. The estimate (143) is valid for the two outer peaks. For the peak at $\Theta_\nu = 40^\circ$, $\overline{V}$ is larger and, accordingly, the resonance energy is slightly smaller. The width of the 1-2 resonance is large and therefore the regions of sizable oscillation probability are more extended in the E_ν direction as compared to the oscillations governed by the 1–3 mixing and splitting.

The resonance energy in the core is $E_{12}^R \approx 0.04\,\text{GeV}$. Therefore for $E_\nu > (0.10\text{–}0.15)\,\text{GeV}$ the 1-2 mixing in the core is substantially suppressed by matter. The peak at $E_\nu \simeq 0.2\,\text{GeV}$ and $\Theta_\nu \simeq 25^\circ$ is due to the parametric enhancement of the oscillations. It corresponds to the realization of the parametric resonance condition when the oscillation half phases equal approximately $\phi_{\text{mantle}} \approx \pi/2$ and $\phi_{\text{core}} \approx 3\pi/2$ (note that the total phase is $\approx 5\pi/2$ and this parametric ridge is attached to the $5\pi/2$ MSW peak in the mantle domain).

4.1.2. Oscillograms for the Inverted Mass Hierarchy. The main change compared to the normal hierarchy is that the 1–3 resonance structure now appears in the antineutrino channel. The level crossing scheme is modified in comparison to NH. In the neutrino channel there is only the 1-2 resonance.

In the approximation of $\Delta m_{21}^2 = 0$, the neutrino oscillograms for the inverted hierarchy coincide with the antineutrino oscillograms for the normal hierarchy and vice versa, provided that Δm_{31}^2 is taken to be the same in both cases [56]: $P_A^{IH} = \overline{P}_A^{NH}$, $\phi_X^{IH} = -\overline{\phi}_X^{NH}$. Therefore $P_{\alpha\beta}^{IH} = \overline{P}_{\alpha\beta}^{NH}$, $\overline{P}_{\alpha\beta}^{IH} = P_{\alpha\beta}^{NH}$. The inclusion of the 1-2 mixing and mass splitting breaks this symmetry.

4.2. CP Violation Effects

4.2.1. Interference and CP Violation. The survival probability P_{ee} does not depend on the CP-violating phase δ neither for oscillations in vacuum nor in matter [57, 58]. This is the consequence of the facts that δ can be removed by transforming to the propagation basis and that ν_e is not affected by this transformation. For oscillations in vacuum, or in matter with symmetric density profiles, the other two survival probabilities, $P_{\mu\mu}$ and $P_{\tau\tau}$, are T-even quantities dependent on δ only through terms proportional to $\cos\delta$ and $\cos 2\delta$ [59]. In contrast to this, for oscillations in a matter with nonsymmetric density profiles, these probabilities also acquire terms proportional to $\sin\delta$ and $\sin 2\delta$.

Introducing the phase $\phi \equiv \arg(A_{e\tilde{2}}^* A_{e\tilde{3}})$ and omitting small terms proportional to $|A_{\tilde{2}\tilde{3}}|^2 = \mathcal{O}(s_{13}^6)$ we obtain

$$P_{\mu e}^\delta = \sin 2\theta_{23} \cos(\phi - \delta) \left|A_{e\tilde{2}} A_{e\tilde{3}}\right|, \tag{144}$$

$$P_{\mu\mu}^\delta = -\sin 2\theta_{23} \cos\delta \cos\phi \left|A_{e\tilde{2}} A_{e\tilde{3}}\right| - D_{23}, \tag{145}$$

$$P_{\mu\tau}^\delta = -\sin 2\theta_{23} \sin\delta \sin\phi \left|A_{e\tilde{2}} A_{e\tilde{3}}\right| + D_{23}, \tag{146}$$

where $D_{23} \equiv (1/2)\sin 4\theta_{23} \cos\delta\, \text{Re}[A_{\tilde{2}\tilde{3}}^* (A_{\tilde{3}\tilde{3}} - A_{\tilde{2}\tilde{2}})]$ is proportional to the small deviation of the 2-3 mixing from maximal one. Notice that D_{23} enters $P_{\mu\mu}^\delta$ and $P_{\mu\tau}^\delta$ with opposite signs while $P_{\mu e}^\delta$ does not depend on D_{23} at all. D_{23} is CP even. The sum of these interference terms is zero.

For the other channels, $P_{\alpha\beta}^\delta = P_{\beta\alpha}^{-\delta}$. For antineutrinos, according to (127), the probabilities have the same form as the corresponding probabilities derived above with a changed sign of δ and the amplitudes computed with the opposite sign of the potential. Thus, the δ-dependent parts in all the

channels are expressed in terms of two combinations of the propagation-basis amplitudes, $|A_{e\tilde{2}}A_{e\tilde{3}}|$ and D_{23}.

4.2.2. Magic Lines and CP Domains. To better assess the effect of δ, one can consider the difference of the oscillation probabilities for two different values of the CP phase $\Delta P^{\mathrm{CP}}_{\alpha\beta}(\delta) \equiv P_{\alpha\beta}(\delta) - P_{\alpha\beta}(\delta_0)$. In practice, this quantifies how well the phase δ fits with some assumed true value δ_0. The structure of the oscillograms for $\Delta P^{\mathrm{CP}}_{\alpha\beta}(\delta)$ can be understood in terms of the grids of magic lines and interference phase lines along which $\Delta P^{\mathrm{CP}}_{\alpha\beta}(\delta) \approx 0$.

For the $\nu_\mu \to \nu_e$ oscillation probability, the equality

$$\begin{aligned}\Delta P^{\mathrm{CP}}_{\mu e}(\delta) &\equiv P_{\mu e}(\delta) - P_{\mu e}(\delta_0) \\ &= P^{\delta}_{\mu e}(\delta) - P^{\delta}_{\mu e}(\delta_0)\end{aligned} \tag{147}$$

is exact and the condition $\Delta P^{\mathrm{CP}}_{\mu e} = 0$ is equivalent to

$$\begin{aligned}&\left|A_{e\tilde{2}}A_{e\tilde{3}}\right|\cos(\phi - \delta) \\ &\quad = \left|A_{e\tilde{2}}A_{e\tilde{3}}\right|\cos(\phi - \delta_0).\end{aligned} \tag{148}$$

This equality is satisfied if at least one of the following three conditions is fulfilled:

$$\begin{aligned}A_{e\tilde{2}}(E_\nu, \Theta_\nu) &= 0, \\ A_{e\tilde{3}}(E_\nu, \Theta_\nu) &= 0, \\ \phi(E_\nu, \Theta_\nu) - \delta_0 &= -[\phi(E_\nu, \Theta_\nu) - \delta] + 2\pi l.\end{aligned} \tag{149}$$

The last condition implies

$$\phi(E_\nu, \Theta_\nu) = \frac{(\delta + \delta_0)}{2} + \pi l. \tag{150}$$

Under the conditions (149), the equality (148) is satisfied identically for all values of δ. In these cases the transition probability does not depend on the CP phase. Since the amplitudes $A_{e\tilde{2}}$ and $A_{e\tilde{3}}$ are complex quantities, these conditions can be satisfied in isolated points of the (Θ_ν, E_ν) plane only. In contrast to this, in the factorization approximation $A_{e\tilde{2}} = A_S$ and $A_{e\tilde{3}} = A_A$ both the conditions are fulfilled along certain lines in the oscillograms. This occurs because the amplitudes A_S and A_A take a 2-flavor form. On the basis of neutrino states where the corresponding 2×2 Hamiltonians are traceless, both A_A and A_S are pure imaginary because of the symmetry of the Earth's density profile [47].

Let us consider the equalities $A_S = 0$ and $A_A = 0$ using the constant density approximation.

(1) The condition $A_S(E_\nu, \Theta_\nu) = 0$ is satisfied when $\sin\phi_S(E_\nu, \Theta_\nu) = 0$, which leads to

$$L(\Theta_\nu) \approx \frac{2\pi n}{\omega^m_{21}}, \quad n = 1, 2, \ldots. \tag{151}$$

At energies $E_\nu \gtrsim 0.5\,\mathrm{GeV}$ which are much higher than the 1-2 mixing MSW resonance in the mantle and in the core of the Earth one has $\omega^m_{21} \approx V$ and the condition (151) becomes

$$L(\Theta_\nu) \simeq \frac{2\pi n}{V}. \tag{152}$$

This expression is energy independent and determines the baselines for which the "solar" contribution to the probability vanishes [61]. In the plane (Θ_ν, E_ν) it represents nearly vertical lines at fixed Θ_ν. There are three solar magic lines which correspond to $n = 1$ (in the mantle domain) $\Theta_\nu \approx 54^\circ$ and $n = 2, 3$ (in the core domain) [61] $\Theta_\nu \approx 30^\circ$ and 12°. The existence of a baseline ($L \approx 7600\,\mathrm{km}$) for which the probability of $\nu_e \leftrightarrow \nu_\mu$ oscillations in the Earth is approximately independent of the "solar" parameters $(\Delta m^2_{21}, \theta_{12})$ and of the CP phase δ was first pointed out in [62] and later discussed in, for example, [61, 63–68]. This baseline was dubbed "magic" in [63].

(2) The atmospheric magic lines are determined by the condition $A_A(E_\nu, \Theta_\nu) = 0$ [61]. Along these lines, the "atmospheric" contribution to the amplitudes of $\nu_\mu \leftrightarrow \nu_e$ and $\nu_\tau \leftrightarrow \nu_e$ transitions vanishes and the probabilities of oscillations involving ν_e or $\bar{\nu}_e$ do not depend on CP phase. In the constant density approximation, the condition $A_A = 0$ is satisfied when $\sin\phi_A = 0$ ($\phi_A = \pi k$, $k = 1, 2, \ldots$) or explicitly

$$L(\Theta_\nu) \approx \frac{2\pi k}{\omega^m_{31}}, \quad k = 1, 2, \ldots. \tag{153}$$

For energies which are not too close to the 1–3 MSW resonance, it reduces to

$$E_\nu \simeq \frac{\Delta m^2_{31} L(\Theta_\nu)}{\left|4\pi k \pm 2VL(\Theta_\nu)\right|}, \tag{154}$$

which corresponds to the bent curves in the (Θ_ν, E_ν) plane. For very large energies, where $\Delta m^2_{31}/2E \ll V$, the atmospheric lines approach the same vertical lines as the solar magic lines (152).

(3) The condition (150) determines the interference phase lines in the (Θ_ν, E_ν) plane. In the constant density approximation $\phi \approx -\phi^m_{31}$. Consequently in the energy range between the two resonances we have

$$\phi^m_{31} \approx \frac{\Delta m^2_{31} L}{4E_\nu} = \phi^0_A, \tag{155}$$

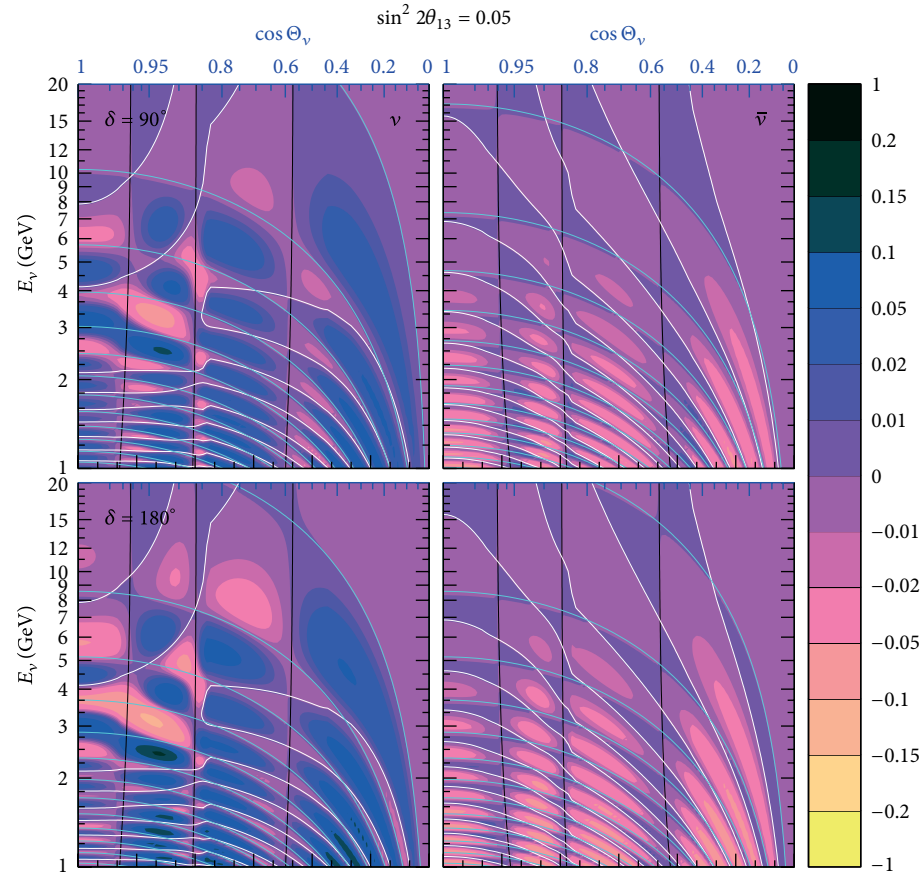

FIGURE 10: Oscillograms for the difference of probabilities $\Delta P^{\mathrm{CP}}_{\mu e}(\delta) = P_{\mu e}(\delta) - P_{\mu e}(\delta_0)$ with $\delta_0 = 0^\circ$. Shown are the solar (black), atmospheric (white), and interference phase condition (cyan) curves from [60].

that is, in the first approximation ϕ does not depend on the matter density. From (150) we then obtain

$$E_\nu = \frac{\Delta m^2_{31} L\left(\Theta_\nu\right)}{4\pi l - 2\left(\delta + \delta_0\right)}. \tag{156}$$

Thus, in the factorization approximation, the conditions (149) and (150) define three sets of lines (grid of magic lines) in the oscillograms (see Figure 10), which play crucial roles in understanding the CP violation effects. Along the lines, the probabilities $P_{\mu e}$, $P_{e\mu}$, $P_{\tau e}$, and $P_{e\tau}$ do not depend on the CP phase in the first order approximation. The other probabilities depend on the phase weakly.

From Figure 10, we can see that the magic lines described above do not coincide exactly with the lines of $\Delta P^{\mathrm{CP}}_{\mu e} = 0$ which bound the CP-domains. Furthermore, interconnections of the latter occur. This is due to the breakdown of the factorization approximation.

4.3. Determination of Hierarchy with Accelerator Experiments. An accelerator neutrino experiment has a fixed baseline which corresponds to a vertical line with the length determined by the available energy spectrum. In the oscillogram of Figure 11 we have included such lines for a handful of accelerator experiments. Furthermore, this energy spectrum is usually peaked at certain energy (or narrow energy range) resulting in the experiment being most sensitive to the oscillation probability at that specific energy. An accelerator neutrino experiment would typically run for several years in neutrinos or antineutrinos before switching polarity and therefore getting information both on $P_{\alpha\beta}$ and $\overline{P}_{\alpha\beta}$. The goal of such a search is to observe in which channel the oscillation probability is suppressed and in which it is enhanced. If a neutrino experiment could run at energy similar to the resonant one and at a baseline of several thousand kilometers, then this determination would be quite simple. However, as can be seen from the oscillogram, accelerator neutrino experiments are confined to relatively shallow trajectories with rather poor oscillatory pattern, and this severely limits their capabilities leading to various degeneracies. In particular, lack of knowledge of the mass hierarchy is part of the famous eightfold degeneracy, which arises as follows. Assume we have access to the values of oscillation probabilities $P_{\mu e}$ and $\overline{P}_{\mu e}$ at a given baseline L and energy E only. Then there exist three types of ambiguities that give rise to the same values of the probabilities in different parts of the parameter space (mixing angles, CP phase, and signs of mass differences).

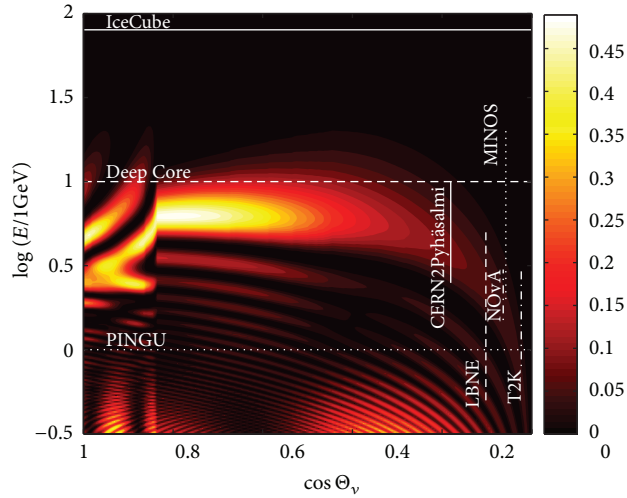

FIGURE 11: Physics reach of the accelerator and atmospheric neutrino experiments. Shown are areas in the oscillogram for $\nu_e \rightarrow \nu_\mu$ channel which can be covered by different accelerator (vertical sections) and atmospheric neutrino experiments (sensitive to the area above the corresponding horizontal lines).

(1) *Sign (hierarchy) degeneracy:* this is the degeneracy due to the unknown neutrino mass hierarchy. Changing the mass hierarchy, it is often possible to find a point in parameter space that predicts the same oscillation probabilities.

(2) *Intrinsic* (θ_{13}, δ) *degeneracy:* for any combination of (θ_{13}, δ), there exists a different combination $(\widehat{\theta}_{13}, \widehat{\delta})$ that also predicts the same oscillation probabilities.

(3) *Octant* (θ_{23}) *degeneracy:* changing the octant of θ_{23} also leads to a degeneracy due to μ-τ symmetry. If θ_{23} is close to maximal, the effects of this degeneracy are less pronounced.

Since each of these degeneracies is twofold, an overall degeneracy is eightfold: $2^3 = 8$. The first two of these degeneracies can be illustrated in a biprobability plot of Figure 12. As follows from this figure, even if both the probabilities (for a given neutrino energy) are known with infinite accuracy, we cannot identify the hierarchy within the pink region.

For known mass hierarchy (e.g., normal one) a given value of θ_{13} fixes ellipse in the plot along which the CP phase varies. Increasing θ_{13} moves the ellipse up and to the right in the plot. Therefore for every point on an ellipse, there will be another ellipse corresponding another value $\theta_{13}^{\text{prime}}$, which crosses this point and therefore $\theta_{13}^{\text{prime}}$ reproduces the same oscillation probabilities. For example, in the left intersection of the black and white ellipse (Figure 12) both combinations of θ_{13} and δ correspond to those precise oscillation probabilities and there are also values of θ_{13} and δ that will reproduce them in the inverted hierarchy. For the right intersection, the intrinsic degeneracy is still present, while the sign degeneracy is resolved. It should be remembered that this type of figure is just an illustration. In real experiment the neutrino energy spans over wide range, the oscillation probabilities would not be exactly known, and strictly this type of consideration becomes invalid.

In order to see how these degeneracies manifest themselves in an experimental setup, we show the oscillation probability $P_{\mu e}$ as a function of the baseline length in Figure 13. While the 295 km baseline is too short for matter effects to be very significant, as the baseline increases matter effects start being more and more important. In particular, when the oscillation phase maximum occurs at an energy similar to that of the matter resonance, as is the case of 7500 km baseline, we can see the enhancement of the transition probability in the neutrino channel for the normal hierarchy and the suppression in the inverted. In a simple two-flavor scenario, the amplitude of $P_{\mu e}$ at the resonance is one by definition in the normal mass hierarchy case. At the same time, the oscillation amplitude in the inverted hierarchy at the same energy is given by

$$\sin^2 2\widetilde{\theta} = \frac{\sin^2 2\theta}{1 + 3\cos^2 2\theta} \simeq \frac{1}{4}\sin^2 2\theta, \tag{157}$$

where the last equality holds for small θ. On the other hand, if the neutrino energy is far below the resonance in order to accumulate a significant oscillation phase, such as in the left and middle panels, then the oscillation amplitude will be effectively given by

$$\sin^2 2\widetilde{\theta} \simeq \sin^2 2\theta \left[1 + \frac{4VE}{\Delta m^2}\cos 2\theta\right]. \tag{158}$$

The reason that the 810 km baseline separates the hierarchies better than the 295 km one is based mainly on the fact that the oscillation maximum can be reached for higher energies due to the longer baseline, and thus, the relative difference between probabilities for the two hierarchies increases. Also note that the oscillation probabilities for the 7500 km baseline are not very dependent on the CP-violating phase δ. This is

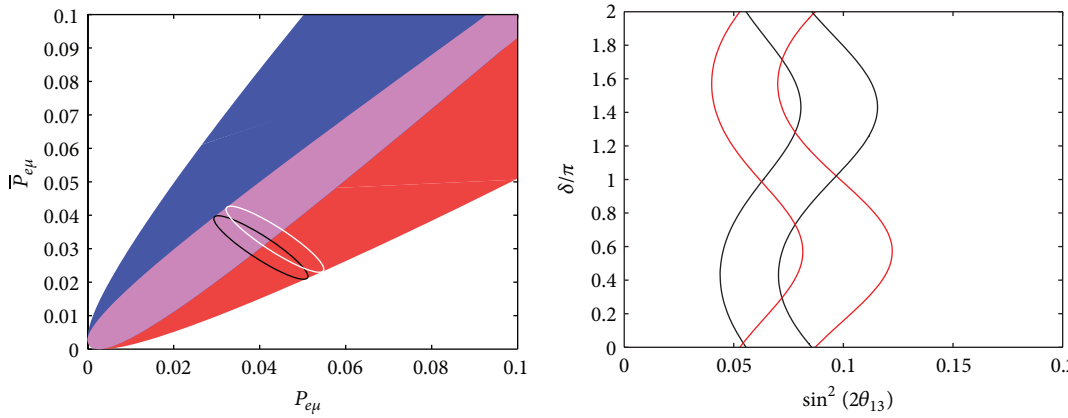

FIGURE 12: Two different illustrations of parameter space degeneracies. Left panel: biprobability plot for $L = 295$ km and $E = 0.65$ GeV. The red band indicates the possible values of the probabilities for normal hierarchy, the blue for inverted, and the pink for the intersection of the two. The black and white ellipses represent the possible values of the probabilities for two different fixed values of θ_{13}. Right panel: probability isocontours of $P_{\mu e}$ (black) and $\overline{P}_{\mu e}$ (red). The values of the probabilities correspond to those of the intersections between the black and white ellipses in the left panel (with the thick lines representing the upper left intersection). The intersections are where the parameter values reproduce the oscillation probabilities for both neutrinos and antineutrinos.

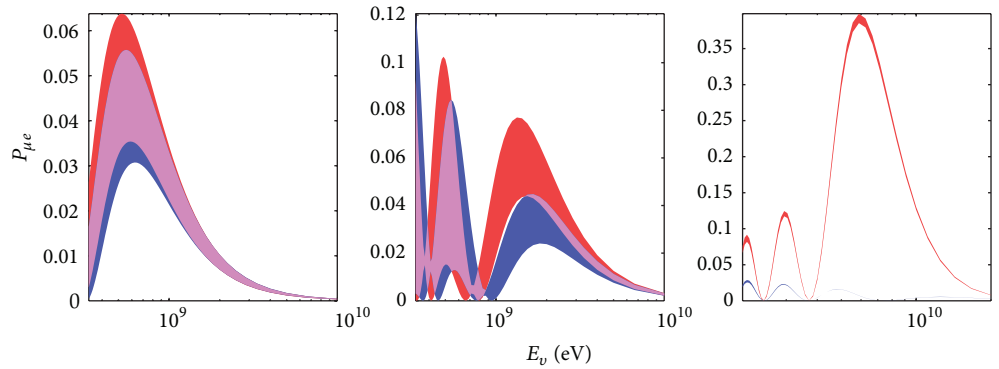

FIGURE 13: The neutrino oscillation probability $P_{\mu e}$ at baselines of 295 (left), 810 (middle), and 7500 km (right) as a function of the neutrino energy. The red (blue) band corresponds to the normal (inverted) mass hierarchy and the band width is obtained by varying the value of δ. The probabilities for $\overline{P}_{\mu e}$ look similar with the hierarchies interchanged. Note the different scales of the axes.

due to the so-called magic baseline effect, which has been discussed before.

In order to successfully determine the neutrino mass hierarchy in a single accelerator experiment, two conditions are of major importance. (1) The baseline must be long enough to allow for a significant value of VE in order to separate the neutrino and antineutrino oscillation probabilities. To separate the mass hierarchy determination from the effects of the CP phase, this separation must be large enough to avoid overlap of the probabilities within the experimental uncertainties. (2) The statistics must be high enough and the systematics low enough in order to make the split statistically significant. The literature contains several proposals for long baseline experiments with baselines of several thousands of kilometers in order to satisfy these conditions. However, as we will discuss later, the large value of θ_{13} also provides us with an opportunity to pin down the value of δ. Such measurements require the presence of interference terms which will be small at the very long baselines, and instead medium long baselines around 1000 km, such as the 810 km baseline shown in Figure 13, may be preferable due to the significant δ dependence of probabilities.

4.3.1. CP Violation Effects and the Mass Hierarchy. Figure 13 shows a significant dependence of the probabilities on the CP-violating phase δ, especially at small baselines. We are mainly interested in the oscillation probability at the first or second oscillation maximum, where an experiment would typically

be placed. In these baselines L the ν_μ-ν_e oscillation probability (the "golden channel") can be expanded in the small quantity $\Delta m^2_{21}L/2E$ which gives [69]

$$P_{e\mu} \approx s^2_{23}P^{2f} + c_{13}\sin 2\theta_{13}\sin 2\theta_{12}\sin 2\theta_{23}\frac{\Delta m^2_{21}}{2EV} \times \sin\left(\frac{VL}{2}\right)\sin\left(\frac{\Delta m^2_{31}L}{4E}\right)\cos\left(\delta - \frac{\Delta m^2_{31}L}{4E}\right), \tag{159}$$

where P^{2f} is the two-flavor oscillation probability discussed earlier. In (159) we have neglected terms of the second (and higher) order in $\Delta m^2_{21}L/2E$ (while the first neglected term is not suppressed by θ_{13}, for the value of θ_{13} measured by reactor experiments the suppression by the solar mass square splitting is about 6 times stronger) as well as the matter effect on Δm^2_{31}. It is the second term that is responsible for creating the band of different oscillation probabilities displayed in Figure 13, and hence, for creating the sign degeneracy in accelerator neutrino experiments. The appearance of the $\sin(VL/2)$ term is an inheritance from the magic baseline oscillations and will vanish the δ-dependent term when $VL = 2\pi$. Furthermore, we can observe that this term contains all of the mixing angles in the same way as the Jarlskog invariant, which is expected due to the CP dependence of the term.

4.4. Determination of Hierarchy with Atmospheric Neutrinos

4.4.1. Neutrino Fluxes. The original flux of atmospheric neutrinos contains incoherent components of ν_e, ν_μ and the corresponding antineutrinos, while the original ν_τ flux is negligible. We introduce Φ^0_e and Φ^0_μ, the electron and muon neutrino fluxes, as well as $\overline{\Phi}^0_e$ and $\overline{\Phi}^0_\mu$, the electron and muon antineutrino fluxes, at the detector in the absence of oscillations. The flavor ratios

$$r \equiv \frac{\Phi^0_\mu}{\Phi^0_e}, \qquad \overline{r} \equiv \frac{\overline{\Phi}^0_\mu}{\overline{\Phi}^0_e} \tag{160}$$

increase with energy.

There is a mild neutrino-antineutrino asymmetry: the neutrino flux $\overline{\Phi}^0_\mu/\Phi^0_\mu \approx 0.8$-$0.9$. All the fluxes (at $E > 1$ GeV) decrease rapidly with energy $\Phi^0_\alpha \propto E^{-k}$, $k = k(E) = 3$–5, and an azimuthal dependence shows up at low energies.

The flux of neutrinos of flavor ν_α at a detector, with oscillations taken into account, is given by

$$\begin{aligned}\Phi_\alpha &= \Phi^0_e P_{e\alpha} + \Phi^0_\mu P_{\mu\alpha} \\ &= \Phi^0_e\left[P_{e\alpha} + r\left(E,\Theta_\nu\right)P_{\mu\alpha}\right], \quad \alpha = e,\mu,\tau.\end{aligned} \tag{161}$$

Similar expressions hold for the antineutrino fluxes. Inserting the analytic expressions for the probabilities (122)–(126), one finds

$$\begin{aligned}\frac{\Phi_e}{\Phi^0_e} &= 1 + \left(rs^2_{23} - 1\right)P_{e\widetilde{3}} + \left(rc^2_{23} - 1\right)P_{e\widetilde{2}} + rP^\delta_{\mu e}, \\ \frac{\Phi_\mu}{\Phi^0_\mu} &\approx 1 - 2s^2_{23}c^2_{23}\left[1 - \mathrm{Re}\left(A^*_{\widetilde{2}\widetilde{2}}A_{\widetilde{3}\widetilde{3}}\right)\right] \\ &\quad - \frac{s^2_{23}}{r}\left(rs^2_{23} - 1\right)P_{e\widetilde{3}} - \frac{c^2_{23}}{r}\left(rc^2_{23} - 1\right)P_{e\widetilde{2}} + P^\delta_{\mu\mu} + \frac{1}{r}P^\delta_{e\mu}, \\ \frac{\Phi_\tau}{\Phi^0_\mu} &\approx 2s^2_{23}c^2_{23}\left[1 - \mathrm{Re}\left(A^*_{\widetilde{2}\widetilde{2}}A_{\widetilde{3}\widetilde{3}}\right)\right] \\ &\quad - \frac{c^2_{23}}{r}\left(rs^2_{23} - 1\right)P_{e\widetilde{3}} - \frac{s^2_{23}}{r}\left(rc^2_{23} - 1\right)P_{e\widetilde{2}} + P^\delta_{\mu\tau} + \frac{1}{r}P^\delta_{e\tau},\end{aligned} \tag{162}$$

where $P_{e\widetilde{3}} \equiv |A_{e\widetilde{3}}|^2$ and $P_{e\widetilde{2}} \equiv |A_{e\widetilde{2}}|^2$ are defined in Section 3.13. In the factorization approximation they correspond to the atmospheric and solar oscillation modes. The δ-dependent terms have been introduced in (144).

Using unitarity relations

$$\begin{aligned}\left|A_{\widetilde{2}\widetilde{2}}\right|^2 &= 1 - \left|A_{\widetilde{2}e}\right|^2 - \left|A_{\widetilde{2}\widetilde{3}}\right|^2 \\ &\approx 1 - \left|A_{\widetilde{2}e}\right|^2 = 1 - P_{e\widetilde{2}},\end{aligned} \tag{163}$$

where the terms proportional to $|A_{\widetilde{3}\widetilde{2}}|^2$ have been neglected we can approximate

$$\mathrm{Re}\left(A^*_{\widetilde{2}\widetilde{2}}A_{\widetilde{3}\widetilde{3}}\right) \approx \sqrt{\left(1 - P_{e\widetilde{3}}\right)\left(1 - P_{e\widetilde{2}}\right)}\cos\psi. \tag{164}$$

Here $\psi \equiv \arg A_{33}A^*_{22}$ is the relative phase between the two amplitudes. For the ν_e flux, we then obtain

$$\begin{aligned}\frac{\Phi_e}{\Phi^0_e} &\approx 1 + \left(rs^2_{23} - 1\right)P_{e\widetilde{3}} + \left(rc^2_{23} - 1\right)P_{e\widetilde{2}} \\ &\quad + r\sin 2\theta_{23}\sqrt{P_{e\widetilde{3}}P_{e\widetilde{2}}}\cos\left(\phi - \delta\right).\end{aligned} \tag{165}$$

The oscillated fluxes satisfy the sum rule

$$\Phi_e + \Phi_\mu + \Phi_\tau = \Phi^0_e + \Phi^0_\mu, \tag{166}$$

which simply reflects the unitarity of transitions and, consequently, conservation of the total flux in oscillations.

The formulas (161) also show the screening effect. Terms with oscillation probabilities driven by the 1-2 and 1–3 mixings appear with the "screening" factors [70, 71]: $P_{e\widetilde{3}}$ with $(rs^2_{23} - 1)$ and $P_{e\widetilde{2}}$ with $(rc^2_{23} - 1)$. The contribution of the "atmospheric mode" vanishes along the line $r(E,\Theta_\nu) = 1/s^2_{23}$, whereas the contribution of the "solar mode" vanishes along $r(E,\Theta_\nu) = 1/c^2_{23}$. For maximal mixing both contributions vanish along the same line, $r(E,\Theta_\nu) = 2$. For the neutrino energies above 0.1 GeV, $r > 1.8$-1.9, and only one of these

contributions can vanish for substantial deviation of the 2-3 mixing from maximal: s^2_{23} or $c^2_{23} < 0.45$. Thus, both the effects of 1-2 and 1–3 mixing turn out to be subleading and the oscillation effects are well described by the first order approximation of 2-3 vacuum oscillations.

In the ν_μ flux, the contributions of the 1-2 and 1–3 modes are suppressed by additional factors s^2_{23}/r and c^2_{23}/r, respectively. There is no suppression of the interference terms, which depend on the CP violation phase. Furthermore, in the ν_e flux the interference term is enhanced by the flux ratio r. There is no suppression of the interference terms of the 1-2 and 1–3 modes in the μ-τ mode.

4.4.2. Sensitivity to Mass Hierarchy. Let us discuss the sensitivity of large water or ice detectors of atmospheric neutrinos to the neutrino mass hierarchy. The ν_μ-like events correspond to interactions $\nu_\mu + N \to \mu + X$, $\overline{\nu}_\mu + N \to \mu^+ + X$ and can be observed as events with muon tracks and hadron cascades. There are also some contributions from ν_τ which produce τ with subsequent decay into μ. The number of ν_μ-like events in the ij-bin in the E_ν-$\cos\theta_z$ plane equals

$$N^{NH}_{ij,\mu} = 2\pi N_A \rho T \int_{\Delta_i \cos\theta_z} d\cos\theta_z \times \int_{\Delta_j E_\nu} dE_\nu V_{\text{eff}}(E_\nu)\, D_\mu(E_\nu, \theta_z), \tag{167}$$

where T is the exposure time, N_A is the Avogadro number, ρ is the density of ice, $V_{\text{eff}}(E_\nu, \theta_z)$ is the effective volume of the detector, and the number density of events per unit time per target nucleon is given by

$$D_\mu(E_\nu, \theta_z) = \left[\sigma^{CC}\left(\Phi^0_\mu P_{\mu\mu} + \Phi^0_e P_{e\mu}\right) + \overline{\sigma}^{CC}\left(\overline{\Phi}^0_\mu \overline{P}_{\mu\mu} + \overline{\Phi}^0_e \overline{P}_{e\mu}\right)\right]. \tag{168}$$

It is assumed here that experiments do not distinguish the neutrino and antineutrino events and corresponding signals are summed up.

The fine-binned distribution of events (166) is shown in Figure 14. For illustration we use the effective volume of PINGU with 22 additional strings [72]. which increases from ~2 Mt at $E_\nu = 2$ GeV to 20 Mt at $E_\nu = 20$ GeV. The pattern of the event number distribution follows the oscillatory picture due to the ν_μ-ν_μ mode of oscillations with a certain distortion in the resonance region. The maxima and minima are approximately along the lines of equal oscillation phases $E_\nu \sim \phi_{32}\Delta m^2_{32}|\cos\theta_z| R_\oplus$ (where $R_\oplus$ is the Earth radius), with distortion in the resonance region $E_\nu = (4\text{–}10)$ GeV. In the high density bins, the number of events reaches 200 and the total number of events is about 10^5.

The expression for the density of events (168) can be written as

$$D^{NH}_\mu = \sigma^{CC}(E_\nu)\,\Phi^0_\mu \left[\left(P_{\mu\mu} + \frac{1}{r}P_{e\mu}\right) + \kappa_\mu\left(\overline{P}_{\mu\mu} + \frac{1}{\overline{r}}\overline{P}_{e\mu}\right)\right], \tag{169}$$

where

$$\kappa_\mu \equiv \frac{\overline{\sigma}^{CC}\overline{\Phi}^0_\mu}{\sigma^{CC}\Phi^0_\mu}. \tag{170}$$

Similarly one can determine the number of events for inverted mass hierarchy. Let us introduce the N-I hierarchy asymmetry for the ij-bin in the (E_ν-$\cos\theta_z$) plane as

$$A^{N\text{-}I}_{\mu,ij} \equiv \frac{N^{IH}_{\mu,ij} - N^{NH}_{\mu,ij}}{\sqrt{N^{NH}_{\mu,ij}}}. \tag{171}$$

The moduli of the asymmetry (171) are the measures of statistical significance of the difference of the number of events for the normal and inverted mass hierarchies: $S_{ij} = |A_{ij}|$.

The strongest effect of hierarchy change is in the strips along the constant phase lines in the energy interval $E_\nu = (4\text{–}12)$ GeV, where these lines are distorted by the matter effect. Here the asymmetry changes sign with the zenith angle, and the number of intervals with the same sign asymmetry increases with the decrease of energy. The $\nu_\tau \to \tau \to \mu$ events can be considered as background events and treated within ~5% systematic errors.

4.4.3. Measurements. According to Figure 14, the hierarchy asymmetry of the ν_μ events has opposite signs in different parts of the oscillogram. Thus, the integration over E_ν and $\cos\theta_z$ substantially reduces the sensitivity to the hierarchy. Due to this, a relatively good reconstruction of the neutrino energy and direction is required to identify the hierarchy. The uncertainties of the reconstruction of energy σ_E and angle σ_θ should be comparable to or smaller than the sizes of the domains with the same sign of the asymmetry. The oscillograms for the reconstructed neutrino energy E^r_ν and angle θ^r_z can be obtained by smearing of the E_ν-$\cos\theta_z$ oscillograms with the reconstruction functions of the width σ_E and angle σ_θ.

Small uncertainties σ_E and σ_θ require rather precise measurements of the energy E_μ and direction θ_μ of the muon, as well as energy of the accompanying hadron cascade E_h. Then the neutrino energy equals $E^r_\nu = E_\mu + E_h$. The reconstruction of the neutrino direction is more involved. In the first approximation, one can use $\theta_\nu \approx \theta_\mu$ with a spread which decreases with energy: $\sigma_\theta \sim A\sqrt{m_p/E_\nu}$ ($A = O(1)$). Knowledge of the hadron cascade energy allows reducing this uncertainty. Further improvements could be possible if some information about geometry of the cascade is available. A possibility to separate (at least partially) the neutrino and antineutrino samples would significantly improve sensitivity to the mass hierarchy, as well as to CP violation.

All this imposes conditions on the detector characteristics. According to Figure 14, the most sensitive region to the hierarchy is around the resonance and above: $E = (5\text{–}15)$ GeV. The number of events in Super-Kamiokande is too small, but (upgraded) ice and underwater detectors of the multimegaton (~10 Mt) scale could collect around the order

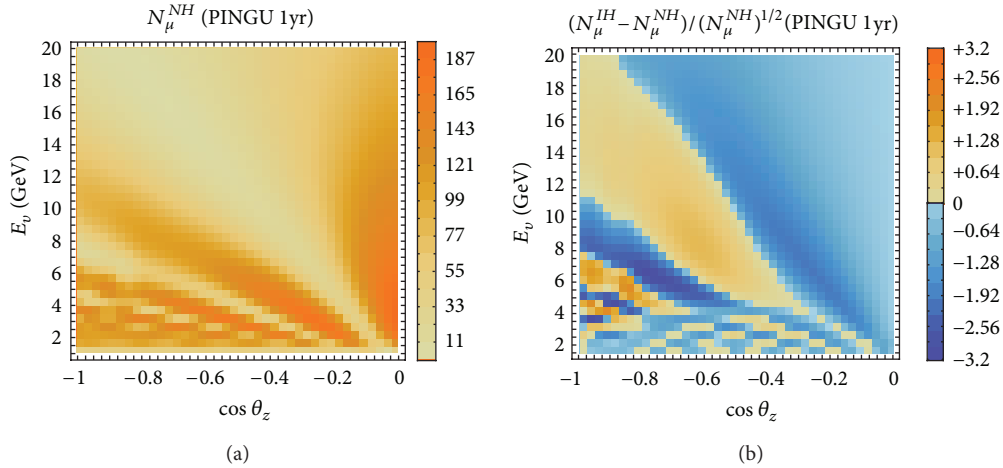

FIGURE 14: Left: the binned distribution of the number of μ events in PINGU after 1 year under the assumption that the neutrino hierarchy is normal. Right: the N-I hierarchy asymmetry of ν_μ events in the E_ν-cos θ_z plane. The absolute value of the asymmetry in a given bin determines the statistical significance of the difference of the numbers of events for the inverted and normal mass hierarchies. Both figures from [56].

of $10^5 \nu_\mu$ events a year in this range so that a high statistics study becomes possible.

A small enough spacing between the PMTs (~10–20 m between strings and 3–5 m in the vertical direction) will allow the reduction of the threshold down to a few GeV and perform reasonably good measurements of the muon and hadron cascade characteristics. Very high statistics will also allow resolving the problem of parameter degeneracy; effects qualitatively similar to the mass hierarchy effect can be obtained by small (within 1σ interval) variations of Δm^2_{32} and θ_{23}. The effect of an unknown CP phase is small.

High statistics would allow resolving the degeneracy problem by selecting specific regions in the E_ν-cosθ_z for the analysis, where effects of Δm^2_{32} are suppressed in comparison to the hierarchy effects or averaged out as a result of specific integration. High statistics also allow performing an analysis of the data using Δm^2_{32} and θ_{23} as fit parameters. This will open a possibility to determine the mass hierarchy and measure these parameters simultaneously.

Note that other experimental techniques using atmospheric neutrinos may also prove valuable for determination of the mass hierarchy. In particular, experiments that can separate neutrinos from antineutrinos on an event basis need a significantly lower number of events to obtain the same sensitivity. Thus, such detectors can be smaller in size as compared to the neutrino telescopes. In this context, a magnetized iron calorimeter, such as the India-based Neutrino Observatory [73], could also provide an important contribution to the determination of mass hierarchy. The capabilities of detectors using charge identification were studied in [74].

4.4.4. Interplay between Accelerator and Atmospheric Neutrinos. The atmospheric neutrino data can also be used to complement the data from accelerator neutrino experiments in order to extract the most information possible. As was demonstrated in [74], the atmospheric neutrino determination of the neutrino mass hierarchy can be significantly affected by the addition of external priors and, in particular, may lead to different sensitivity to the neutrino mass hierarchy in the cases of true normal or inverted hierarchy. However, once external input on the neutrino oscillation parameters is included by considering also other experiments, the room to mimic the true oscillation pattern in the wrong hierarchy becomes much more restricted and the sensitivity to the hierarchy increases. Adding the accelerator experiments' own sensitivity to the mass hierarchy, a measurement may be possible even for the current generation of accelerator experiments by the addition of detector capable of lepton charge identification. This has been discussed in [75] and the prospects of using a magnetized iron calorimeter detector to augment the current generation of accelerator experiments are a 2–4σ determination of the mass hierarchy within 10 years of data taking, depending on the true value of the oscillation parameters and the characteristics of the detector.

5. Discussion and Conclusions

In this paper, we have described the effects of neutrino propagation in matter relevant to experiments with atmospheric and accelerator neutrinos and aimed at the determination of the neutrino mass hierarchy and CP violation. Thus, to a large extent, we have focused on neutrino propagation in the Earth matter.

(1) At relatively low energies, the dominant effect of neutrino interactions with matter is the elastic forward scattering, which is described by an effective potential. Neutrino evolution in matter is then described by a Schrödinger-like equation including this effective potential. The potential differences for neutrinos of different types influence the flavor evolution of the system of mixed neutrinos. In the majority of realistic

situations, neutrinos propagate in normal (unpolarized nonrelativistic) matter with nearly constant or slowly changing density.

(2) Matter modifies the neutrino flavor mixing and changes the eigenvalues of the Hamiltonian of propagation. This is equivalent to a modification of the dispersion relations of neutrinos. The influence of matter on mixing of neutrinos has a resonance character. At energies or densities for which the eigenfrequency of the neutrino system with mixing $\omega_{ij} = \Delta^2_{ij}/2E$ equals approximately the eigenfrequency of the medium $2\pi/l_0$, the mixing in matter becomes maximal. Large mixing shifts the position of the resonance to lower values of the potential. At usual densities, there are two resonances related to the two mass squared differences Δm^2_{21} and Δm^2_{31} between the neutrino mass eigenstates. The resonances are realized in oscillation channels involving electron neutrinos.

(3) In many practical situations, knowledge of neutrino mixing in matter and the eigenstates of the Hamiltonian in matter allows finding the results of the neutrino flavor evolution immediately. This includes neutrino oscillations in matter with constant density and also adiabatic conversion of neutrinos, where the averaged oscillation results can be written down immediately. In the nonaveraged case, the problem is reduced to finding the oscillation phase (integrating the energy splittings over distance). In this sense the Nature has implemented the most (computationally) simple setups. The very convenient presentation of mixing in matter can be obtained as series expansion in the ratio of the two mass squared differences, r_Δ (perturbative diagonalization of the effective Hamiltonian), which allows to understanding a number of subtle results. The simplest and physically transparent description of dynamics of neutrino flavor evolution can be obtained in the propagation basis (in the case of the standard parameterization). In this basis, the CP-violating phase and 2-3 mixing do not influence the evolution and the amplitudes of transitions do not depend on δ or θ_{23}. The dependence on these parameters appears as a result of projecting the states of the propagation basis back to the flavor states at production and detection. In many practical cases the 3ν evolution can be reduced to evolution of two neutrino systems with certain corrections.

(4) There are two practically important cases: (i) neutrino propagation in matter with constant or nearly constant density and (ii) neutrino propagation in matter with slowly (adiabatically) changing density.

(5) In the case of constant density, flavor evolution has a character of oscillations with parameters determined by mixing and mass splitting in matter. The oscillations are an effect of a phase difference increase in the course of neutrino propagation. The resonance enhancement of oscillations is realized in an energy region around E_R. If the density is approximately constant, then the results can be obtained by using perturbation theory in the deviation of the density distribution from a constant one. The accuracy improves if the density profile is symmetric with respect to the middle point of the neutrino trajectory, as is realized for neutrinos crossing the Earth. A simple and rather precise semianalytical description of neutrino oscillations in matter with varying density can be obtained in the limits of small density, $V < \Delta m^2_{ij}/2E$, and high density, $V \gg \Delta m^2_{ij}/2E$. The latter gives a very accurate description of neutrino flavor evolution in the Earth at $E >$ (8–10) GeV.

(6) In a medium with slowly changing density, adiabatic conversion takes place. This effect is related to the change of mixing in matter due to density change. Adiabaticity implies that there are no transitions among the eigenstates of the instantaneous Hamiltonian during propagation. The strongest flavor transformation is realized when the initial density is much larger, and the final one is much lower than the resonance density. In this case, the initial state (and due to adiabaticity, the state at any other moment of evolution) practically coincides with one of the eigenstates. Therefore, oscillation effects are absent and nonoscillatory flavor conversion takes place. This is realized for supernova neutrinos and approximately for high energy solar neutrinos. In general, if the initial mixing is not strongly suppressed, an interplay of adiabatic conversion and oscillations occurs. Adiabatic transformations are also realized for neutrinos with energy $\leq$ 1 GeV propagating in the mantle of the Earth. In particular, this means that the oscillation depth at the detector is determined by mixing at the surface of the Earth and not by mixing at average density. Until now, the mater effects have been observed in solar neutrinos and, indirectly, in atmospheric neutrinos and there is good chance that they will be observed by new generation of the accelerator and atmospheric neutrino experiments.

(7) Strong flavor transition can be realized without enhancement of mixing. This occurs in matter with periodic or quasiperiodic density change when the parametric resonance condition is fulfilled. For small mixing strong transition requires a large number of periods. A similar enhancement can take place in matter with several layers of different densities. Here the enhancement occurs when a certain correlation between the oscillation phases in each layer and amplitudes of oscillations determined by mixing is present. The case of a medium with 3 layers (1.5 periods) is of practical interest for neutrinos crossing both the mantle and the core of the Earth. For a multilayer medium two conditions must be satisfied to have strong transitions: the amplitude (collinearity) and the phase conditions.

(8) For neutrinos crossing a small amount of matter, such as accelerator experiments with baselines up to

$(1\text{-}2) \cdot 10^3$ km, the column density of matter is small and, according to the minimal width condition, the matter effect on oscillations is small regardless of energy, vacuum mass splitting, and neutrino mixing. Furthermore, if the oscillation phase is small, then mimicking of vacuum oscillations occurs.

(9) A comprehensive description of the neutrino flavor transitions in the Earth is given in terms of neutrino oscillograms of the Earth. After the recent determination of the 1–3 mixing, the structure of oscillograms is well fixed. The salient features of oscillograms at high energies (due to 1–3 mixing) are the MSW resonance peak in the mantle domain, three parametric ridges, and the MSW peak in the core domain. At low energies (due to 1-2 mixing), there are three peaks, due to the MSW resonance, and the parametric ridge. The positions of all these and other structures are determined by the generalized phase and amplitude conditions. In the case of normal mass hierarchy, the resonance peaks induced by the 1–3 mixing are in the neutrino channels. For inverted mass hierarchy they are in the antineutrino channels. This is the foundation for determining the neutrino mass hierarchy. The resonance structures due to the 1-2 mixing are always in the neutrino channels, since the sign of the small mass square difference has been fixed.

(10) The CP properties of the oscillograms (their dependence on CP phase) are determined by the CP domains, areas in which the CP violation effect has the same sign. The borders of these domains are approximately determined by the grids of the magic lines (solar and atmospheric magic lines) and the lines where the oscillation phase condition is fulfilled.

(11) Measurements of matter effects in neutrino oscillations provide a good opportunity to determine the neutrino mass hierarchy. The 1-2 ordering has been determined due to the matter effect of solar neutrinos. The 1–3 ordering can be identified by studying the matter effects in accelerator and atmospheric neutrino experiments. There is a good chance that future studies of the atmospheric neutrinos with multimegaton underwater (ice) detectors will be able to establish the mass hierarchy. With a threshold of a few GeV, these detectors will be sensitive to the resonance region (~ 6–10) GeV, where the difference of probabilities for the normal and inverted mass hierarchies is maximal. The challenges here are the accuracy of reconstruction of the neutrino energies and directions. Integration over the energy and angle, as well as summation of neutrino and antineutrino signals, diminishes the sensitivity to the hierarchy. Another problem is the degeneracy of the hierarchy effects with the effects of other neutrino parameters, in particular with Δm^2_{32} and θ_{32}.

(12) In accelerator experiments, many of the problems mentioned above are absent. However, existing and proposed accelerator experiments will cover only peripheral regions of oscillograms where enhancement of oscillations is very weak and oscillatory structures are rather poor. As a consequence the problem of degeneracy here is even more severe.

References

[1] L. Wolfenstein, "Neutrino oscillations in matter," *Physical Review D*, vol. 17, no. 9, pp. 2369–2374, 1978.

[2] V. Barger, K. Whisnant, S. Pakvasa, and R. J. N. Phillips, "Matter effects on three-neutrino oscillations," *Physical Review D*, vol. 22, no. 11, pp. 2718–2726, 1980.

[3] S. Mikheev and A. Y. Smirnov, "Resonance amplification of oscillations in matter and spectroscopy of solar neutrinos," *Soviet Journal of Nuclear Physics*, vol. 42, pp. 913–917, 1985.

[4] S. P. Mikheyev and A. Y. Smirnov, "Resonant amplification of ν oscillations in matter and solar-neutrino spectroscopy," *Il Nuovo Cimento C*, vol. 9, no. 1, pp. 17–26, 1986.

[5] S. Mikheev and A. Y. Smirnov, "Neutrino oscillations in a variable density medium and neutrino bursts due to gravitational collapse of stars," *Soviet Physics—JETP*, vol. 64, pp. 4–7, 1986.

[6] D. Notzold and G. Raffelt, "Neutrino dispersion at finite temperature and density," *Nuclear Physics*, vol. B307, pp. 924–936, 1988.

[7] B. Pontecorvo, "Mesonium and anti-mesonium," *Soviet Physics—JETP*, vol. 6, p. 429, 1957.

[8] Z. Maki, M. Nakagawa, and S. Sakata, "Remarks on the unified model of elementary particles," *Progress of Theoretical Physics*, vol. 28, no. 5, pp. 870–880, 1962.

[9] B. Pontecorvo, "Neutrino experiments and the problem of conservation of leptonic charge," *Soviet Physics—JETP*, vol. 26, pp. 984–988, 1968.

[10] F. J. Botella, C. S. Lim, and W. J. Marciano, "Radiative corrections to neutrino indices of refraction," *Physical Review D*, vol. 35, no. 3, pp. 896–901, 1987.

[11] S. Esposito and G. Capone, "Neutrino propagation in a medium with a magnetic field," *Zeitschrift fur Physik*, vol. C70, pp. 55–64, 1996.

[12] H. Nunokawa, V. B. Semikoz, A. Y. Smirnov, and J. W. F. Valle, "Neutrino conversions in a polarized medium," *Nuclear Physics B*, vol. 501, no. 1, pp. 17–40, 1997.

[13] A. Lobanov and A. Studenikin, "Neutrino oscillations in moving and polarized matter under the influence of electromagnetic fields," *Physics Letters B*, vol. 515, no. 1-2, pp. 94–98, 2001.

[14] L. Wolfenstein, "Effects of matter on neutrino oscillations," in *Proceedings of the Long-Distance Neutrino Detection (Neutrinos '78)*, West Lafayette, Ind, USA, 1978.

[15] L. Wolfenstein, "Neutrino oscillations and stellar collapse," *Physical Review D*, vol. 20, no. 10, pp. 2634–2635, 1979.

[16] E. K. Akhmedov and A. Wilhelm, "Quantum field theoretic approach to neutrino oscillations in matter," *Journal of High Energy Physics*, http://arxiv.org/abs/1205.6231.

[17] N. Cabibbo, "Summary talk," in *Proceedings of the 10th International Workshop on Weak Interactions and Neutrinos*, 1985.

[18] H. A. Bethe, "Possible explanation of the solar-neutrino puzzle," *Physical Review Letters*, vol. 56, no. 12, pp. 1305–1308, 1986.

[19] A. Bueno, M. Campanelli, and A. Rubbia, "Physics potential at a neutrino factory: can we benefit from more than just detecting muons?" *Nuclear Physics B*, vol. 589, no. 3, pp. 577–608, 2000.

[20] M. Freund, "Analytic approximations for three neutrino oscillation parameters and probabilities in matter," *Physical Review D*, vol. 64, no. 5, Article ID 053003, 2001.

[21] G. L. Fogli, E. Lisi, A. Marrone, D. Montanino, A. Palazzo, and A. M. Rotunno, "Global analysis of neutrino masses, mixings, and phases: entering the era of leptonic CP violation searches," *Physical Review D*, vol. 86, no. 1, Article ID 013012, 10 pages, 2012.

[22] A. Y. Smirnov and S. Mikheev, "Neutrino oscillations in matter with varying density," in *Quarks '86: Proceedings of the Seminar Tbilisi*, 1986.

[23] J. Bouchez, M. Cribier, W. Hampel, J. Rich, M. Spiro, and D. Vignaud, "Matter effects for solar neutrino oscillations," *Zeitschrift für Physik C*, vol. 32, no. 4, pp. 499–511, 1986.

[24] V. K. Ermilova, V. A. Tsarev, and V. A. Chechin, "Parametric enhancement of neutrino oscillations in matter," *Fiz. [Short Notices of the Lebedev Institute]*, vol. 5, p. 26, 1986.

[25] A. Messiah, "Treatment of electron-neutrino oscillations in solar matter: the MSW effect," in *Proceedings of the Moriond Workshop, Massive Neutrinos*, 1986.

[26] E. Lisi, A. Marrone, D. Montanino, A. Palazzo, and S. T. Petcov, "Analytical description of quasivacuum oscillations of solar neutrinos," *Physical Review D*, vol. 63, Article ID 093002, 2001.

[27] A. Friedland, "On the evolution of the neutrino state inside the sun," *Physical Review D*, vol. 64, Article ID 013008, 2001.

[28] A. Y. Smirnov, D. N. Spergel, and J. N. Bahcall, "Is large lepton mixing excluded?" *Physical Review D*, vol. 49, no. 3, pp. 1389–1397, 1994.

[29] H. Minakata and H. Nunokawa, "Inverted hierarchy of neutrino masses disfavored by supernova 1987A," *Physics Letters B*, vol. 504, no. 4, pp. 301–308, 2001.

[30] S. J. Parke, "Nonadiabatic level crossing in resonant neutrino oscillations," *Physical Review Letters*, vol. 57, no. 10, pp. 1275–1278, 1986.

[31] W. C. Haxton, "Analytic treatments of matter-enhanced solar-neutrino oscillations," *Physical Review D*, vol. 35, no. 8, pp. 2352–2364, 1987.

[32] S. T. Petcov, "On the non-adiabatic neutrino oscillations in matter," *Physics Letters B*, vol. 191, no. 3, pp. 299–303, 1987.

[33] P. C. de Holanda, W. Liao, and A. Y. Smirnov, "Toward precision measurements in solar neutrinos," *Nuclear Physics B*, vol. 702, no. 1-2, pp. 307–332, 2004.

[34] C. Lunardini and A. Y. Smirnov, "The minimum width condition for neutrino conversion in matter," *Nuclear Physics B*, vol. 583, no. 1-2, pp. 260–290, 2000.

[35] H. Minakata and H. Nunokawa, "Measuring leptonic CP violation by low energy neutrino oscillation experiments," *Physics Letters B*, vol. 495, no. 3-4, pp. 369–377, 2000.

[36] E. K. Akhmedov, "Matter effects in oscillations of neutrinos traveling short distances in matter," *Physics Letters*, vol. 503, pp. 133–139, 2001.

[37] E. K. Akhmedov, "Resonance enhancement of the neutrino spin precession in matter and the solar neutrino problem," *Soviet Journal of Nuclear Physics*, vol. 48, pp. 382–383, 1988.

[38] P. I. Krastev and A. Y. Smirnov, "Parametric effects in neutrino oscillations," *Physics Letters B*, vol. 226, no. 3-4, pp. 341–346, 1989.

[39] V. Ermilova, V. Tsarev, and V. Chechin, "Buildup of neutrino oscillations in the earth," *Letters to Jounal of Experimental and Theoretical Physics*, vol. 43, p. 453, 1986.

[40] Q. Y. Liu and A. Y. Smirnov, "Neutrino mass spectrum with $\nu\mu \rightarrow \nu s$ oscillations of atmospheric neutrinos," *Nuclear Physics B*, vol. 524, no. 3, pp. 505–523, 1998.

[41] Q. Liu, S. Mikheyev, and A. Y. Smirnov, "Parametric resonance in oscillations of atmospheric neutrinos?" *Physics Letters B*, vol. 440, pp. 319–326, 1998.

[42] S. T. Petcov, "Diffractive-like (or parametric-resonance-like?) enhancement of the Earth (day-night) effect for solar neutrinos crossing the Earth core," *Physics Letters B*, vol. 434, no. 3-4, pp. 321–332, 1998.

[43] M. Chizhov, M. Maris, and S. Petcov, "On the oscillation length resonance in the transitions of solar and atmospheric neutrinos crossing the earth core," http://arxiv.org/abs/hep-ph/9810501.

[44] M. V. Chizhov and S. T. Petcov, "New conditions for a total neutrino conversion in a medium," *Physical Review Letters*, vol. 83, no. 6, pp. 1096–1099, 1999.

[45] M. V. Chizhov and S. T. Petcov, "Enhancing mechanisms of neutrino transitions in a medium of nonperiodic constant-density layers and in the Earth," *Physical Review D*, vol. 63, no. 7, Article ID 073003, 2001.

[46] E. K. Akhmedov, M. Maltoni, and A. Y. Smirnov, "1–3 leptonic mixing and the neutrino oscillograms of the Earth," *Journal of High Energy Physics*, vol. 0705, p. 077, 2007.

[47] E. Akhmedov, P. Huber, M. Lindner, and T. Ohlsson, "T violation in neutrino oscillations in matter," *Nuclear Physics B*, vol. 608, no. 1-2, pp. 394–422, 2001.

[48] E. Lisi and D. Montanino, "Earth regeneration effect in solar neutrino oscillations: an analytic approach," *Physical Review D*, vol. 56, no. 3, pp. 1792–1802, 1997.

[49] A. Takamura and K. Kimura, "Large non-perturbative effects of small on neutrino oscillation and CP violation in matter," *Journal of High Energy Physics*, vol. 0601, p. 053, 2006.

[50] S. Toshev, "On T violation in matter neutrino oscillations," *Modern Physics Letters A*, vol. 6, p. 455, 1991.

[51] E. K. Akhmedov, R. Johansson, M. Lindner, T. Ohlsson, and T. Schwetz, "Series expansions for three avor neutrino oscillation probabilities in matter," *Journal of High Energy Physics*, vol. 0404, p. 078, 2004.

[52] P. Lipari, unpublished, 1998.

[53] T. Ohlsson and H. Snellman, "Neutrino oscillations with three flavors in matter: applications to neutrinos traversing the Earth," *Physics Letters B*, vol. 474, no. 1-2, pp. 153–162, 2000.

[54] M. Jacobson and T. Ohlsson, "Extrinsic CPT violation in neutrino oscillations in matter," *Physical Review D*, vol. 69, Article ID 013003, 2004.

[55] T. Kajita, "Atmospheric neutrinos," *New Journal of Physics*, vol. 6, pp. 1–34, 2004.

[56] E. K. Akhmedov, S. Razzaque, and A. Y. Smirnov, "Mass hierarchy, 2-3 mixing and CP-phase with Huge Atmospheric Neutrino Detectors," http://arxiv.org/abs/1205.7071.

[57] T.-K. Kuo and J. T. Pantaleone, "T nonconservation in three neutrino oscillations," *Physics Letters B*, vol. 198, p. 406, 1987.

[58] H. Minakata and S. Watanabe, "Solar neutrinos and leptonic CP violation," *Physics Letters B*, vol. 468, no. 3-4, pp. 256–260, 1999.

[59] H. Yokomakura, K. Kimura, and A. Takamura, "Overall feature of CP dependence for neutrino oscillation probability in arbitrary matter profile," *Physics Letters B*, vol. 544, no. 3-4, pp. 286–294, 2002.

[60] E. Kh. Akhmedov, M. Maltoni, and A. Yu. Smirnov, "Neutrino oscillograms of the Earth: effects of 1-2 mixing and CP-violation," *Journal of High Energy Physics*, vol. 2008, no. 6, article 072, 2008.

[61] A. Y. Smirnov, "Neutrino oscillations: what is "magic" about the magic baseline?" http://arxiv.org/abs/hep-ph/0610198.

[62] V. Barger, D. Marfatia, and K. Whisnant, "Breaking eight fold degeneracies in neutrino CP violation, mixing, and mass hierarchy," *Physical Review D*, vol. 65, Article ID 073023, 2002.

[63] P. Huber, "CP, T and CPT violation in future long baseline experiments," *Journal of Physics G*, vol. 29, no. 8, pp. 1853–1856, 2003.

[64] P. Huber and W. Winter, "Neutrino factories and the "magic" baseline," *Physical Review D*, vol. 68, no. 3, Article ID 037301, 2003.

[65] R. Gandhi, P. Ghoshal, S. Goswami, P. Mehta, and S. U. Sankar, "Earth matter effects at very long baselines and the neutrino mass hierarchy," *Physical Review D*, vol. 73, no. 5, Article ID 053001, 2006.

[66] A. Blondel, "Future neutrino oscillation facilities: physics priorities and open issues," *Acta Physica Polonica B*, vol. 37, no. 7, pp. 2077–2113, 2006.

[67] P. Huber, M. Lindner, M. Rolinec, and W. Winter, "Optimization of a neutrino factory oscillation experiment," *Physical Review D*, vol. 74, no. 7, Article ID 073003, 2006.

[68] S. K. Agarwalla, S. Choubey, and A. Raychaudhuri, "Unraveling neutrino parameters with a magical beta-beam experiment at INO," *Nuclear Physics B*, vol. 798, no. 1-2, pp. 124–145, 2008.

[69] A. Cervera, A. Donini, M. B. Gavela et al., "Golden measurements at a neutrino factory," *Nuclear Physics B*, vol. 579, no. 1-2, pp. 17–55, 2000.

[70] O. L. G. Peres and A. Yu. Smirnov, "Testing the solar neutrino conversion with atmospheric neutrinos," *Physics Letters B*, vol. 456, no. 2-4, pp. 204–213, 1999.

[71] E. K. Akhmedov, A. Dighe, P. Lipari, and A. Y. Smirnov, "Atmospheric neutrinos at super-Kamiokande and parametric resonance in neutrino oscillations," *Nuclear Physics B*, vol. 542, no. 1-2, pp. 3–30, 1999.

[72] D.F. Cowen and D. Grants, *Private communications*.

[73] INO, India-Based Neutrino Observatory, http://www.ino.tifr.res.in/ino/.

[74] S. T. Petcov and T. Schwetz, "Determining the neutrino mass hierarchy with atmospheric neutrinos," *Nuclear Physics B*, vol. 740, no. 1-2, pp. 1–22, 2006.

[75] M. Blennow and T. Schwetz, "Identifying the neutrino mass ordering with INO and NOvA," *Journal of High Energy Physics*, http://arxiv.org/abs/1203.3388.